

1972

*S. J. Bauer*

**SANDIA REPORT** SAND84-2618 • Unlimited Release • UC-32  
Printed April 1985

# **SANCHO**

## **A Finite Element Computer Program for the Quasistatic, Large Deformation, Inelastic Response of Two-Dimensional Solids**

Charles M. Stone, Raymond D. Krieg, Zelma E. Beisinger

Prepared by  
Sandia National Laboratories  
Albuquerque, New Mexico 87185 and Livermore, California 94550  
for the United States Department of Energy  
under Contract DE-AC04-76DP00789

SAND84-2618  
Unlimited Release  
Printed April 1985

**SANCHO**

**A Finite Element Computer Program for the Quasistatic, Large  
Deformation, Inelastic Response of Two-Dimensional Solids**

Charles M. Stone  
Raymond D. Krieg  
Zelma E. Beisinger

Applied Mechanics Division I  
Sandia National Laboratories  
Albuquerque, New Mexico 87185

**Abstract**

SANCHO is a finite element computer program designed to compute the quasistatic, large deformation, inelastic response of planar or axisymmetric solids. Finite strain constitutive theories for plasticity, volumetric plasticity, and metallic creep behavior are included. A constant bulk strain, bilinear displacement isoparametric finite element is employed for the spatial discretization. The solution strategy used to generate the sequence of equilibrium solutions is a self-adaptive dynamic relaxation scheme which is based on explicit central difference pseudo-time integration and artificial damping. A master-slave algorithm for sliding interfaces is also implemented. A theoretical development of the appropriate governing equations and a description of the numerical algorithms are presented along with a user's guide which includes several sample problems and their solution.

## ACKNOWLEDGEMENT

The authors acknowledge the early technical contributions and continued interest in this work by S. W. Key. Significant contributions to the development of SANCHO were made by several of the early users. H. S. Morgan, 1521, performed numerous checks of the constitutive models; L. J. Branstetter, 1524, and D. S. Preece, 1521, used early versions of the program and provided constructive comments regarding its performance. The efforts of these individuals are gratefully acknowledged.

## CONTENTS

	Page
Acknowledgements . . . . .	4
List of Figures . . . . .	6
List of Tables . . . . .	9
1 Introduction . . . . .	11
2 Mechanics . . . . .	13
2.1 Equations of Equilibrium . . . . .	13
2.2 Strain and Strain Rate . . . . .	16
2.3 Incremental Form of the Problem . . . . .	17
2.4 Spatial Discretization . . . . .	21
2.5 Dynamic Relaxation . . . . .	24
2.6 Sliding Interface Model . . . . .	30
3 Constitutive Relations . . . . .	33
3.1 Stress Flux Relations . . . . .	33
3.2 Plasticity . . . . .	34
3.3 Volumetric Plasticity . . . . .	40
3.4 Metallic Creep . . . . .	47
3.5 Material State Parameter . . . . .	52
3.6 Finite Strain Mechanical Properties . . . . .	52
4 SANCHO User Instructions . . . . .	57
4.1 Problem Definition . . . . .	58
4.2 Material Property Specification . . . . .	65
4.3 Boundary Condition Specification . . . . .	69
5 External File Definition . . . . .	77
6 Example Problems . . . . .	83
6.1 Free Thermal Expansion . . . . .	83
6.2 Pressurized Infinite Cylinder . . . . .	86
6.3 Stress Relaxation . . . . .	88
6.4 WIPP Benchmark II . . . . .	91
7 References . . . . .	96

## FIGURES

		Page
Figure 1:	The body $\mathcal{V}$ with surface tractions $s^k$ on the boundary $\mathcal{S}^1$ and a prescribed motion on the boundary $\mathcal{S}^2$ . An interboundary $\mathcal{S}^0$ with a unit normal vector $n^k$ is pictured.	15
Figure 2:	The cross-section of an axisymmetric body with a four node isoparametric quadrilateral element. The isoparametric coordinates range between minus one and plus one.	22
Figure 3:	The basis function $\phi^1$ obtained from considering the contributions of the respective interpolation functions from each element surrounding nodal point 1.	23
Figure 4:	A model equilibrium iteration sequence in a multidimensional configuration space of nodal point positions developed with dynamic relaxation showing convergence at load step $n + 1$ . The straight line path from $n$ to the last step calculated from dynamic relaxation is the interval over which the stress $t_{rs}^{n+1}$ is evaluated using the real time step $\Delta t$ .	27
Figure 5:	Schematic of Master-Slave Slideline Algorithm. Dashed Line Represents Deformed Location of Slave Node 1.	31
Figure 6:	The typical behavior of a ductile metal bar loaded first in uniaxial tension followed by uniaxial compression. The straight line approximation is characterized as an elastic modulus $E$ , a yield stress $t_0$ , a strain hardening modulus $E_t$ , and a hardening parameter $\beta$ where kinematic hardening is obtained with $\beta = 0$ , isotropic hardening is obtained with $\beta = 1$ , and a linear combination of the two is obtained for $\beta$ between zero and one.	35

	Page
Figure 7:	The pressure versus volume strain behavior for a porous material. Unloading is assumed to occur elastically with a modulus of $K_0$ . . . . . 43
Figure 8:	The standard uniaxial tension test. . . . . 53
Figure 9:	The results of the standard uniaxial tension test expressed in terms of the Cauchy stress versus the logarithmic strain. . . . . 54
Figure 10:	The standard hydrostatic compression test . . . . . 54
Figure 11:	The results of the standard hydrostatic compression test expressed in terms of the Cauchy pressure versus the logarithmic bulk strain. . . . . 55
Figure 12:	Example of the use of a single PHISTORY card to define multiple time histories through the use of the delay time, $t_d$ . . . . . 69
Figure 13:	Mixed stress and displacement boundary condition where the node remains free to move in a direction parallel to a line with inclination $\psi$ . . . . . 72
Figure 14a:	Geometry and Boundary Conditions for Free Thermal . . . . . 84
Figure 14b:	Comparison of SANCHO Results and Theory for Free Thermal Expansion Example . . . . . 84
Figure 15:	Comparison of SANCHO Results with Theory for an Internally Pressurized Infinite Cylinder. . . . . 86
Figure 16a:	Model and Boundary Conditions for the Stress Relaxation Example Problem. . . . . 88
Figure 16b:	Stress History for the Relaxation Problem . . . . . 89
Figure 17:	Problem Definition for the WIPP Benchmark II Isothermal Problem [28]. . . . . 92

	Page
Figure 18. Mesh Used by SANCHO for the WIPP Benchmark II Isothermal Problem. . . . .	93
Figure 19. Closure Results for the WIPP Benchmark II [28]. . . . .	94

**TABLES**

	Page
TABLE 1. Summary of Keywords and Input. . . . .	74

## 1 INTRODUCTION

Since the early 1970's, there has been a growing interest in the solution of nonlinear quasistatic engineering problems. The desire to obtain nonlinear solutions was motivated by the national energy crisis and the need to design and develop new and efficient sources of energy. Typical design practice, where the body was to remain elastic throughout service, was no longer acceptable in many of these applications, so the detailed response of the body in the nonlinear regime was required. Leading the way in this area were the designers of nuclear power plants. In particular, the design of the breeder reactor did a great deal to promote the regular use of nonlinear analysis in design. The elevated temperature operating regime coupled with the extended operating life made the use of nonlinear analysis techniques a necessity for component design.

The development and use of numerical techniques to analyze quasistatic nonlinear behavior was largely confined to researchers at universities. However, a few general purpose finite element computer programs, such as MARC[1] and ADINA[2], were available to industry during this period. The general purpose computer program provided the user with an extensive element library and the ability to solve a wide range of problems. Most of the computer programs were based on an implicit formulation which required the formation and subsequent factorization of a stiffness matrix. The generally adopted nonlinear solution scheme was some form of the Newton-Raphson method. The use of a modified or unmodified Newton-Raphson method places a burden on the analyst to decide when to update the stiffness matrix to prevent the solution from diverging. This requires the analyst to have some knowledge in advance about the solution response. One of the drawbacks to the use of a general purpose program was the inefficiency inherent in maintaining generality. Special purpose programs to solve particular classes of problems do not have this limitation. The special purpose program generally was limited to a very small element library while still employing the implicit solution algorithm.

SANCHO is a special purpose, finite element program that has been developed in response to some of the perceived drawbacks with existing finite element software for nonlinear analysis. SANCHO was developed to solve the quasistatic, large deformation, inelastic response of two dimensional solids. The element library is based on a bilinear isoparametric quadrilateral with a constant bulk strain. The equilibrium solution strategy uses an iterative scheme designed around a self-adaptive dynamic relaxation algorithm. The iterative scheme is based on explicit central difference pseudo-time integration with artificial damping. The code is explicit in nature so that no stiffness matrix is formed or factorized which reduces the amount of computer storage necessary for execution. The explicit nature of the program also makes it attractive for future vectorization on vector processing machines. The code has a standard material model interface which is used with the three material models incorporated within the code. A finite strain elastic-plastic strain hardening model, a volumetric plasticity model, and a metallic creep material model are presently included. A sliding interface capability, based on a master-slave algorithm, is also incorporated within SANCHO. The user-oriented data input scheme is based on keyword descriptors and utilizes a free field reader for ease of data entry. SANCHO is designed to work with a separate mesh generation program such as QMESH [3] and to write a data file which can be used by various plot codes for graphical post processing of the data. The capability to write a restart file is also provided.

In the following sections of this report, a description of the theory and computational methods used in SANCHO is given. A description of the constitutive models is also provided. An input guide for use of the program is included along with several sample problems.

## 2 MECHANICS

Although SANCHO is designed to handle only axisymmetric and planar problems, the theoretical treatment in this section is general for the sake of brevity and completeness. The treatment of continuum mechanics found in Truesdell and Toupin [4] is used.

### 2.1 Equations of Equilibrium

A body  $\mathcal{V}$  occupies a finite region of Euclidean space and is subjected to prescribed body forces and surface tractions. The body undergoes the motion  $x^i = \chi^i(X^\alpha, t)$ . Particles of the body are identified by the coordinates  $X^\alpha$ . They are referred to as material coordinates, and the relation of the particles to the coordinates  $X^\alpha$  does not change in time. The places in space which the particles occupy during the motion are identified by the coordinates  $x^i$ . The function  $\chi^i$  describes the motion of the particles  $X^\alpha$  through space as a function of time  $t$ . It is the motion  $\chi^i$  which is sought.

The place occupied by the body at  $t = 0$  is taken as the reference configuration. In this configuration, the body is assumed to be strain free, though not necessarily stress free. Only material coordinates  $X^\alpha$  which coincide with the spatial coordinates  $x^i$  in the reference configuration are considered. Thus, in the reference configuration,  $\chi^i(X^\alpha, 0) \equiv X^\alpha$ .

The problem is stated in terms of the principle of virtual work. The differential form

$$\delta\pi = \int_{\mathcal{V}} t^{km} \delta x_{k,m} dv - \int_{\mathcal{V}} \rho f^k \delta x_k dv - \int_{\mathcal{S}} s^k \delta x_k da \quad (1)$$

is to vanish at all points along the path of motion for all variations  $\delta x_k$  satisfying the displacement boundary conditions on  $\mathcal{P}^2$ . The integration is performed over the current configuration of the body  $\mathcal{V}$ , where  $\rho$  is the mass density in that configuration,  $t^{km}$  is the Cauchy stress—the stress in the current configuration, and  $s^k$  is the surface traction which is acting on  $\mathcal{P}^1$ . The comma in  $x_{k,m}$  denotes covariant differentiation.

The divergence theorem is employed to display the equilibrium equations. In anticipation of using the finite element method to generate approximate solutions, the case where  $\delta x_{k,m}$  is only piecewise continuous is considered. Interior surfaces where the discontinuities of  $\delta x_{k,m}$  occur are denoted by  $\mathcal{P}^0$ . Only surfaces  $\mathcal{P}^0$  which are stationary with respect to the material are considered. The situation is pictured in Figure 1 where  $n_k$  is the normal to  $\mathcal{P}^0$  and the symbols + and - denote the respective sides of the surface. The result is

$$\begin{aligned}
 & - \int_{\mathcal{V}} (t^{km},m + \rho f^k) \delta x_k dv + \int_{\mathcal{P}^0} (t_+^{km} - t_-^{km}) n_m \delta x_k da \\
 & + \int_{\mathcal{P}^1} (t^{km} n_m - s^k) \delta x_k da = 0 \quad . \quad (2)
 \end{aligned}$$

The differential form will vanish if and only if the respective integrands vanish. The resulting expressions are equilibrium

$$t^{km},m + \rho f^k = 0 \quad \text{in } \mathcal{V} \quad , \quad (3)$$

the jump condition at a contact discontinuity

$$(t_+^{km} - t_-^{km})n_m = 0 \quad \text{on } \mathcal{P}^0, \quad (4)$$

and the traction boundary conditions

$$t^{km}n_m = s^k(t) \quad \text{on } \mathcal{P}^1. \quad (5)$$

The displacement boundary conditions are

$$\chi^i(X^\alpha, t) = \kappa^i(t) \quad \text{on } \mathcal{P}^2. \quad (6)$$

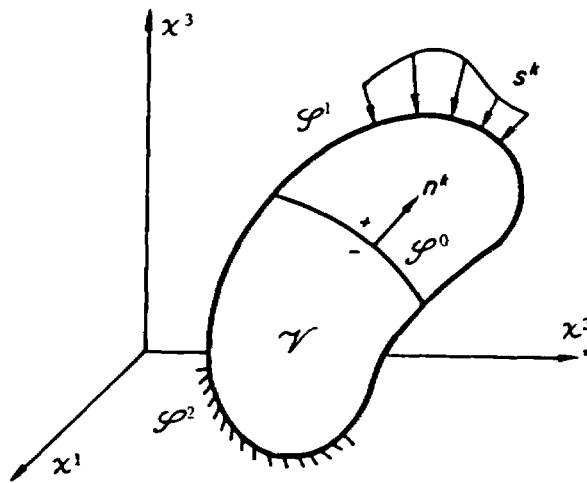


Figure 1. The body  $\mathcal{V}$  with surface tractions  $s^k$  on the boundary  $\mathcal{P}^1$  and a prescribed motion on the boundary  $\mathcal{P}^2$ . An interboundary  $\mathcal{P}^0$  with a unit normal vector  $n^k$  is pictured.

It is important to realize that these equations are completely general and applicable for arbitrarily large deformations.

## 2.2 Strain and Strain Rate

In finite deformations there are many strain measures which are useful. The majority of them can be computed from the deformation gradient  $F_{\alpha}^k$  defined by

$$F_{\alpha}^k \equiv \frac{\partial x^k}{\partial X^{\alpha}} (X^{\beta}, t) \quad . \quad (7)$$

The left Cauchy-Green tensor is computed from the deformation gradient as

$$B^{km} = F_{\alpha}^k F_{\beta}^m G^{\alpha\beta} \quad . \quad (8)$$

The quantity  $G^{\alpha\beta}$  is the metric tensor in the coordinates of the reference configuration. The velocity  $v^k$  is defined as

$$v^k(X^{\alpha}, t) \equiv \frac{\partial x^k}{\partial t} (X^{\alpha}, t) \quad . \quad (9)$$

The stretching is given by

$$d_{km} = \frac{1}{2} (v_{k,m} + v_{m,k}) \quad , \quad (10)$$

with the spin by

$$w_{km} = \frac{1}{2} (v_{k,m} - v_{m,k}) \quad . \quad (11)$$

In the constitutive models which follow, only the left Cauchy-Green tensor  $B^{km}$  and the stretching  $d_{km}$  are used as strain and strain rate measures, respectively. There are additional strain and strain rate variables which could be introduced but they are not needed here. Further reference to them can be found in Truesdell and Toupin [4].

### 2.3 Incremental Form of the Problem

The notion of an incremental solution is fundamental to many of the methods for finding a motion  $\chi^1(X^\alpha, t)$  which generates a stress history in equilibrium with the applied loads. It is assumed that at time  $t_n$ , the stress  $t_{rs}^n$  satisfies the equilibrium Equations (3), (4), and (5); and the stress  $t_{rs}^n$  is the result of integrating the constitutive models with the strain histories derived from the known motion up to  $t_n$ . The prescribed loads are incremented to time  $t_{n+1}$  and a predictor/corrector method is introduced to find the new configuration  $\chi_{n+1}^1 = \chi^1(X^\alpha, t_{n+1})$  which has all the equilibrium properties which were deemed necessary at  $t_n$  and accuracies

acceptable to the constitutive model evaluation. To indicate the incremental quantities a  $\Delta$  is used. For example,  $\Delta t = t_{n+1} - t_n$ ,  $\Delta t_{rs} = t_{rs}^{n+1} - t_{rs}^n$ , etc.

A basic assumption which underlies most incremental treatments, including the one here, but which is rarely stated is that the motion between  $x_n^i$  and  $x_{n+1}^i$  is linear. As a consequence, the incremental velocity given by  $v_{n+1/2}^i = \Delta x^i / \Delta t$  is constant over the time increment. Equilibrium is tested in the configuration at  $t_{n+1}$  which is a trial configuration until equilibrium is established. To do this, the stresses at  $t_{n+1}$  must be evaluated. Following Hughes and Winget [5], a one parameter family of configurations is introduced

$$x_{n+\alpha}^i = (1 - \alpha)x_n^i + \alpha x_{n+1}^i \quad (12)$$

The gradient  $h_{ij}$  of  $u_i = \Delta x^i$  with respect to  $x_{n+\alpha}^j$  is given by

$$h_{ij} = u_{i,j} \quad (13)$$

From this gradient, the strain increment  $e_{ij}$  is given by

$$e_{ij}(\alpha) = \frac{1}{2} \left[ h_{ij} + h_{ji} + (1 - 2\alpha)h_{ki}h_{kj} \right] \quad (14)$$

Thus,  $e_{ij}(0)$  is the Green-St. Venant strain increment,  $e_{ij}(1)$  is the Signorini strain increment, and

$$e_{ij} \left( \frac{1}{2} \right) = \Delta t d_{ij}^{n+1/2} = \text{sym} \left( \frac{\partial u_i}{\partial x^j_{n+1/2}} \right) \quad (15)$$

Without the need for further linearization, the configuration halfway between  $n$  and  $n+1$  is selected for evaluating the stretching, spin, and for computing  $\Delta t$ . The midpoint configuration is optimal in the sense that no quadratic terms are needed to accurately evaluate  $(dx^i dx^i)_{n+1} - (dx^i dx^i)_n$ .

The terms in the co-rotational derivative involving the spin  $w^{rk}$  used in the constitutive equations are for the purposes of taking into account rigid body rotations of a material point relative to the spatial coordinates  $x^i$ . In incremental form they are an orthogonal rotation through an incremental angle. Hughes and Winget have provided a modern account of this process and have provided a direct way to evaluate the orthogonal rotation matrix  $R_{ij}$  from the spin  $w_{ij}$ . Thus,

$$R_{ij} = \left( \delta_k^i - \Delta t \frac{1}{2} w_k^i \right)^{-1} \left( g_{kj} + \Delta t \frac{1}{2} w_{kj} \right) \quad (16)$$

Half angle trigonometric formulas are used to get the square root of  $[R]$ ;  $R_{ij} = R_{ik}^{1/2} R_{kj}^{1/2}$ . With these constructions, the constitutive models can be integrated over the increment from  $n$  to  $n+1$ . First, the stress  $t_{rs}^n$  and the applicable state variables  $\alpha_{rs}^n$  are rotated to  $n + 1/2$  by

$$\bar{t}_{rs}^{n+1/2} = \left( R^{1/2} \right)_r \left( R^{1/2} \right)_s t_{ij}^n \quad (17)$$

and

$$\bar{\alpha}_{rs}^{n+1/2} = \left( R^{1/2} \right)_r \left( R^{1/2} \right)_s \alpha_{ij}^n \quad (18)$$

Using  $\bar{d}_{rs}^{n+1/2}$  and  $\Delta t$ , the constitutive equations are integrated and new stresses  $\bar{t}_{rs}^{n+1/2}$  and state variables  $\bar{\alpha}_{rs}^{n+1/2}$  are obtained. These are then rotated from  $n + 1/2$  to  $n + 1$  by the same process as in Equations (17) and (18). This process of mid-interval constitutive evaluation is also used by Hallquist [6] and Biffle [7].

Of particular importance is the integration of the constitutive equations from time  $n$  to  $n + 1$ . The plasticity model is integrated from  $n$  to  $n + 1$  assuming the stretching is constant which is consistent with Equation (17). For a constant stretching path, the integration is quite accurate, extremely reliable, and independent of the specific value for the time interval  $\Delta t$  [8-10]. The creep model is also integrated from  $n$  to  $n + 1$  assuming the stretching is constant. The creep equations, however, are not nearly as easy to integrate numerically. They are mathematically "stiff" equations. Only with considerable effort and great expense can they be numerically integrated with conventional methods from time  $n$  to  $n + 1$ . To overcome this stiffness, a semianalytic integration is used. Domains in stress and strain rate space are identified where various nearby differential equations with exact solutions are applicable. The solution path over a time step may remain within a single domain or may pass through two or more domains requiring the solutions to two or more of the differential equations to be applied, one after the other over the time step. In this way, arbitrarily large strain or time intervals can be accurately and reliably taken. An absolute maximum of seven subincrements are required so that computational time is not excessive. This approach,

while conceptually straightforward, is highly tailored to the constitutive model at hand. The present approach to constitutive equations uncouples stability and accuracy in their evaluation from selection of the time step size used in load incrementing schemes with their attendant equilibrium iteration, cf., Bushnell [11]. This approach contrasts with that where  $\Delta t$  in the constitutive integration scheme corresponds to the  $\Delta t$  used in incrementing the load. If this coupling is pursued, many numerical schemes can be developed. Argyris, Vaz and William [12] have documented a number of these and have provided the guidance necessary for their successful use.

## 2.4 Spatial Discretization

The treatment up to this point has been in terms of an arbitrary body undergoing an arbitrary motion. Of interest now are the axisymmetric and plane strain problems. Because the planar case may be obtained from the axisymmetric case by moving the symmetry axis arbitrarily far off, only the axisymmetric problem is discussed. No attempt is made to do the axisymmetric problem in general, but rather a specific element with specific interpolation functions is introduced from the outset.

If cylindrical coordinates,  $r$ ,  $\theta$ ,  $z$  are introduced, an axisymmetric body can be characterized by a cross-section in the  $r$ - $z$  plane which, when revolved about the  $z$ -axis, generates the body. Such a cross-section with a quadrilateral element is pictured in Figure 2 (such an element is frequently called a "ring element"). As indicated in Figure 2, the element is a four node isoparametric element [13]. Thus, if  $y^\alpha$  represents the value of the function  $y$  at the node with index  $\alpha$ , and  $\phi^\alpha$  represents the interpolation function at the node, the function  $y$  is described within the element by

$$y = \sum_{\alpha=1}^4 y^\alpha \phi^\alpha(a,b) \quad (19)$$

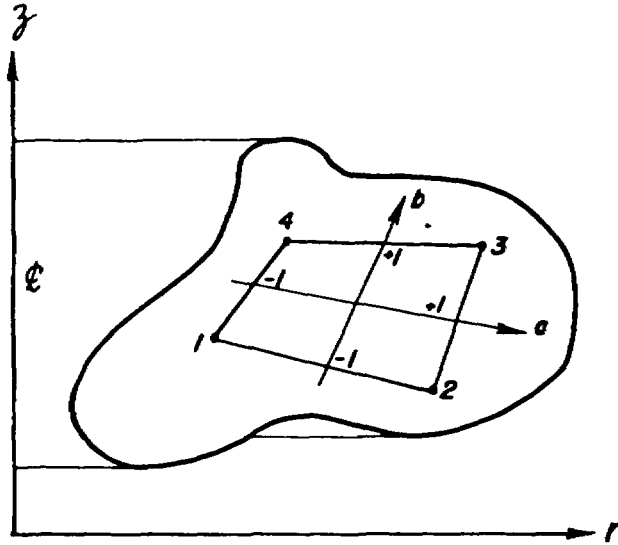


Figure 2. The cross-section of an axisymmetric body with a four node isoparametric quadrilateral element. The isoparametric coordinates range between minus one and plus one.

where the bilinear isoparametric interpolation functions are given by

$$\phi^1 = (1 - a)(1 - b)/4 \quad \phi^2 = (1 + a)(1 - b)/4 \quad (20)$$

$$\phi^3 = (1 - a)(1 + b)/4 \quad \phi^4 = (1 + a)(1 + b)/4$$

When all the elements around node 1 are considered, the basis function obtained from the interpolation functions in each element can be pictured. Figure 3 shows the result for this case. As can be seen in Figure 3, the basis functions obtained in this manner have only piecewise continuous gradients along the element boundaries. As a result, implicit in the finite element equations which result from this choice of basis functions is an approximation to the jump conditions (4) along each element interface.

When the basis functions are introduced into the principle of virtual work and the variations taken, a discrete form of the differential Equations (3), (4), and (5) is obtained as

$$\{T\} = \{F\} \quad (21)$$

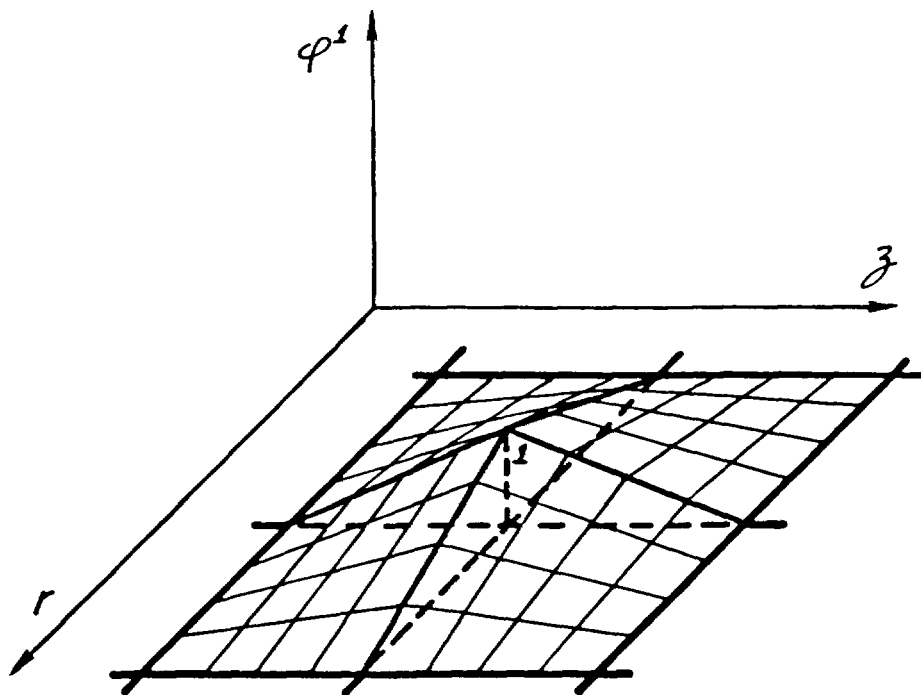


Figure 3. The basis function  $\phi^1$  obtained from considering the contributions of the respective interpolation functions from each element surrounding nodal point 1.

where, with no sums on the index k.

$$\{T\} = \int_V t^{km} \phi_{k,m}^\alpha dv \quad , \text{ a vector}$$

$$\{F\} = \int_V \rho f^k \phi_k^\alpha dv + \int_J s^k \phi_k^\alpha da \quad , \text{ a vector.}$$

This is a discrete statement which requires the divergence of the stress field  $\{T\}$  to be in equilibrium with the prescribed body forces and surface tractions  $\{F\}$ .

The integrals for  $\{T\}$  over each element are performed numerically using Gaussian quadrature rules. A  $2 \times 2$  integration is used to evaluate the area integral. In the process, a constant bulk strain is used. This may be viewed as a 1 point integration of the volumetric strain energy and a  $2 \times 2$  integration of the deviatoric strain energy, [14-16].

## 2.5 Dynamic Relaxation

As a solution strategy for statics problems, dynamic relaxation involves first converting the equilibrium equations into equations of motion by adding an acceleration term, second, introducing an artificial damping, and finally, integrating forward in time from initial conditions until the transient dynamic response has damped out to the static result with equilibrium satisfied. An early introduction of the idea is given by Otter, et al. [17], but a more recent work which summarizes all of the significant contributions on the topic since then is Underwood [18]. In reference [18], considerable detail is presented about dynamic relaxation and its use in nonlinear problems. Additional information on dynamic relaxation can be found in the paper by Papadrakakis [19].

Dynamic relaxation is attractive for three reasons: it is vectorizable, it is versatile, and it is reliable. Because it can be made explicit, it is highly vectorizable for modern digital calculations. In an explicit form, it is ideal for dealing with large deformations, finite strains, and inelastic material behavior. It is reliable in that if the algorithm converges and equilibrium is achieved, then the solution will be good.

To produce a dynamic problem, an acceleration term is added to the equilibrium Equation (3). Thus,

$$t^{km},m + \rho f^k = r \frac{\partial^2 u^k}{\partial \tau^2} \quad (22)$$

where  $r$  is a spatially varying density selected to minimize the number of steps needed to reach equilibrium and  $\tau$  is a pseudo-time scale connected with the dynamic relaxation but distinct from real time  $t$ . The acceleration term is discretized the same way that it would be in a true dynamics calculation, [20]. This leads to the discrete system

$$[M]\{\ddot{q}\} = \{F\} - \{T\} \quad (23)$$

where

$$\{q\} = \dot{u}^{k\alpha}(\tau) \quad , \text{ a vector } ,$$

$$[M] = \int_V r \phi_k^\alpha dv \quad , \text{ a diagonal matrix } .$$

At time  $t_n$ , equilibrium is satisfied so that  $\{T\}_n = \{F\}_n$ . A new solution is initiated by incrementing the load to its value at time  $t_{n+1}$ . In general, equilibrium will not be satisfied, so that the imbalance is represented by the acceleration term:

$$[M]\{\ddot{q}\} = \{F\}_{n+1} - \{T\}_{n+1} \quad (24)$$

damping is then chosen to provide critical damping for the lowest frequency. This expression is

$$\delta = 1 - 4\omega_0\omega_1/(\omega_0 + \omega_1)^2 \quad . \quad (26)$$

The range on  $\delta$  is (0.1). A stability analysis on this set of explicit equations produces a critical pseudo-time step given by

$$\Delta\tau_c = 2/\delta^{1/2}(\omega_0 + \omega_1) \quad . \quad (27)$$

If the problem were linear so  $\omega_0$  and  $\omega_1$  are fixed, then the number of time steps required to reduce the amplitude by a factor of ten would be

$$N \approx 1.15 \omega_1/\omega_0 \quad (28)$$

From Equation (28), it is seen that any action to reduce the ratio  $\omega_1/\omega_0$  speeds convergence.

From the linear problem and a uniform mesh of dimension  $h$ , the maximum frequency  $\omega_1$  is given by

$$\omega_1 = 2 c/h \quad . \quad (29)$$

Here  $c$  is the uniaxial strain "sound speed" given by  $[(\lambda + 2\mu)/r]^{1/2}$  where  $r$  is the pseudo-density used in Equation (22). While the problem is nonlinear in the large, as equilibrium is approached at the end of each load step, the behavior is linear. With Equation (29), the condition on  $\Delta\tau$  is essentially the well known Courant-Friedrich-Levy condition which says that  $\Delta\tau$  can be no larger than the time it takes for information to travel between the "closest" two nodes in the mesh.

On the basis of these observations, the concept of mesh homogenization is introduced. The densities  $r$  are selected element-by-element to give the same transit time across each element, regardless of the size of the element. Thus, information about equilibrium imbalance is transmitted uniformly over the mesh. This process gives the lowest possible value to the maximum frequency  $\omega_1$ , the goal being to minimize the ratio  $\omega_1/\omega_0$  in Equation (28).

The fundamental frequency  $\omega_0$  is continuously estimated using an approximate Rayleigh quotient, [18]. At each step  $i$  in the dynamic relaxation, a new estimate  $(\omega_0)_i$  is computed from Equation (30).

$$(\omega_0)_i = (\{q\}_i^T [K]_{loc} \{q\}_i / \{q\}_i^T [M] \{q\}_i)^{1/2}, \quad (30)$$

Where  $[K]_{loc}$  is a diagonal stiffness matrix whose  $j^{\text{th}}$  component is computed from

$$[K]_{loc} |_j = (\{T\}_i |_j - \{T\}_{i-1} |_j) / (\Delta\tau \{P\}_{i-1/2} |_j) \quad (31)$$

With each estimate of the fundamental frequency, a new value of the damping  $\delta$  is computed. This has the virtue that the lowest active mode will be found in the event that the fundamental mode is not participating. [18].

## 2.6 Sliding Interface Model

There are several numerical approaches for modeling sliding interface behavior which allow arbitrary values of the friction coefficient. One method requires the use of a thin finite element which has a special constitutive model to approximate gap and friction behavior [21]. A second approach uses Lagrange multipliers to impose gap closure constraints and frictional stick-slip conditions [1]. SANCHO utilizes a third method, the master-slave approach for slideline kinematics [22].

In the master-slave concept, the nodes on the designated slave surface are required by the algorithm to lie on the master surface. Any sliding or slip must occur along the master surface. In turn, nodal forces from the slave surface are removed and applied to the master surface nodes. This transfer of forces maintains equilibrium at the interface. The tangential shear or friction force as well as the determination of slip or no slip is incorporated in this process of the transfer of forces to the master surface. In SANCHO the nodal forces are computed by the divergence of stresses over the element. Therefore nodal forces can be used in conjunction with a Mohr-Coulomb model which usually employs shear and normal stresses.

The operation of the scheme can be demonstrated in the following example where slave node I lies between master nodes M and N, as shown in Figure 5. The algorithm determines whether node I has crossed the straight line drawn between M and N. If node I has penetrated the master surface, then the normal force ( $R_N$ ) and tangential force ( $R_T$ ) at node I are determined. The coefficient of friction,  $\mu$ , is used in conjunction with  $R_N$  to determine the threshold value for slip,  $\mu R_N$ . If  $R_T$  is less than  $\mu R_N$ , then no slip occurs and both the values  $R_N$  and  $R_T$  are transferred to the

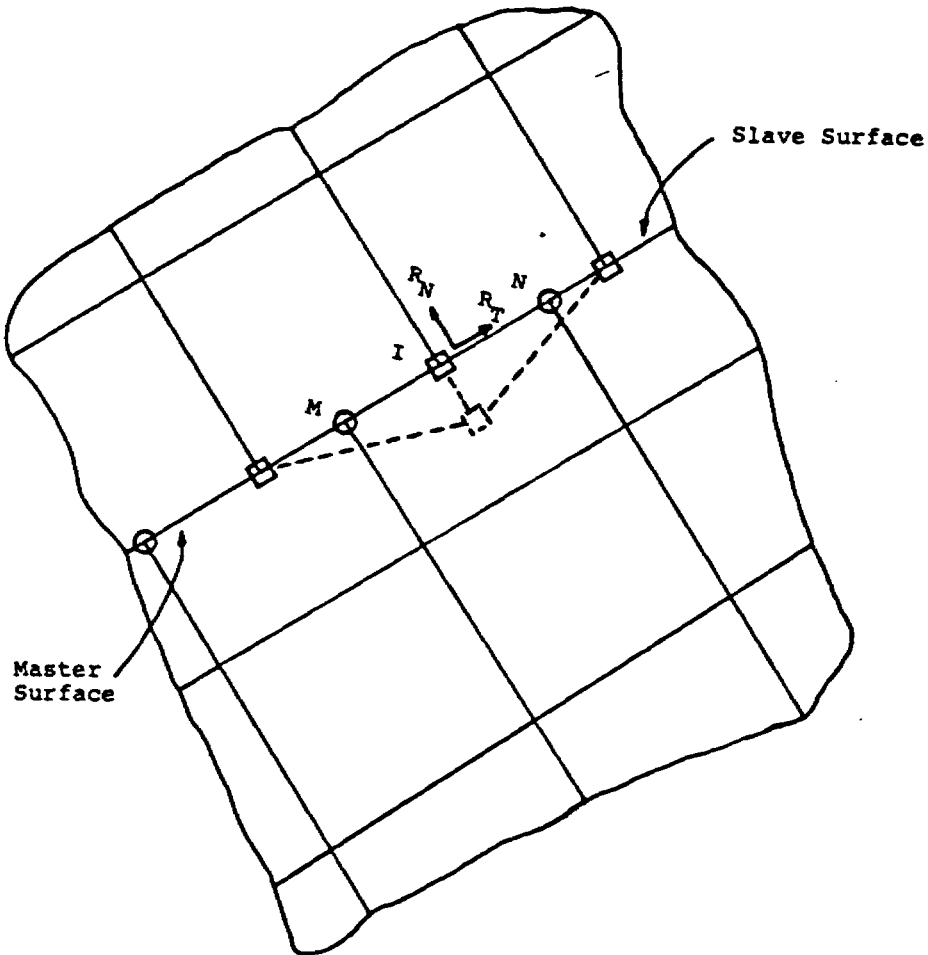


Figure 5. Schematic of Master-Slave Slideline Algorithm Dashed Line Represents Deformed Location of Slave Node I.

master surface nodes using an area weighting procedure. The slave node I is assigned the displacement of the corresponding point on the master surface. However, if  $R_T$  is greater than  $\mu R_N$ , then slip can occur. The tangential force  $R_T$  is reset to its maximum allowable value of  $\mu R_N$ . The forces  $R_N$  and  $R_T$  are again transferred to the master nodes, but only the normal master surface displacement is applied to the slave node. The tangential displacement is not specified, but is allowed to seek a new equilibrium position along the slideline. This procedure is incorporated within the iterative framework of SANCHO and is found to produce reliable results.

Inclusion of friction, however, does have a disadvantage. The expense of computing with finite values of friction is increased in many cases over computations where the coefficient is zero or the two surfaces are fixed.

Incorporated within the slideline model is the capability for two surfaces initially in contact to separate at a prescribed stress level and for two distinct surfaces to contact each other and remain in contact during deformation. The user is allowed to specify the separation stress level and to specify the separation tolerance within which both surfaces are assumed to be in contact. The separation stress is computed at the slave surface Gauss point closest to the slave node.

### 3 CONSTITUTIVE RELATIONS

#### 3.1 Stress Flux Relations

When a material in a given class is subjected to finite strains, it will often exhibit unique behavior which distinguishes it from the other materials in the class. Finite strain relations will frequently be more detailed and more specific because of this. The experimental procedures necessary for large strain characterization are correspondingly more difficult and can easily be misinterpreted. As a result, it is more difficult to write relations characteristic of a large class of materials. Since the majority of relations included here are generalizations of infinitesimal relations, the reader must be cautioned as to their general applicability to every material. The stress relations used here are fairly simple. They are meant to capture the fundamental behavior of materials with as few parameters as possible. Any of them could be easily generalized or expanded.

Many stress relations are developed in the reference configuration and as a result the second Piola-Kirchhoff stress  $T^{\alpha\beta}$  is used. Since the equations of motion used here are based on the Cauchy stress  $t^{km}$ , the second Piola-Kirchhoff stresses generated in these relations must be converted with the relation:

$$t^{km} = |\det F_{\gamma}^i|^{-1} F_{\alpha}^k T^{\alpha\beta} F_{\beta}^m \quad (32)$$

where  $F_{\alpha}^k$  is the deformation gradient.

Several stress and strain measures are found in finite strain plasticity models currently in use. While use of different variables make the models appear at first to be different, on closer examination they are

all very nearly the same and differ only in detail—Key, Biffle, and Krieg [23]. It is clear, however, that the rates used for stress and strain, in particular, must be compatible.

The main subject of the research, however, concerns the choice of a stress flux measure. We have decided to retain the use of the corotational flux. The corotational flux of the Cauchy stress is related linearly through a tangent modulus to the stretching, also known as the rate of deformation tensor. Thus,

$$\dot{\tau}^{rs} = \dot{t}^{rs} - g^{rk} w_{km} \dot{t}^{ms} - g^{sk} w_{km} \dot{t}^{mr} \quad (33)$$

where  $w_{km}$  is the spin defined in Equation (11).

This relation for the stress flux is used for all the material models. The constitutive relations are all written in terms of the stress flux.

### 3.2 Plasticity

Plasticity is characteristic of ductile metals. Figure 6 shows behavior which is typical of a metal bar loaded first in uniaxial tension followed by uniaxial compression. The straight line representation in Figure 6 is an idealization of this behavior. This is the approximation which results from the plasticity relations employed here and taken from Goel and Malvern [24]. The approach taken here, with the exception of the kinematic hardening which is included here, is widely used in finite difference method "hydrocodes." The stress flux is given by  $\dot{\tau}^{rs} = C^{rsmn} d_{mn}$ .

When the behavior is elastic  $C^{rsmn}$  is the isotropic tensor,  $\lambda g^{rs} g^{mn} + 2\mu g^{rm} g^{sn}$ , where  $\lambda$  and  $\mu$  are the Lamé parameters.

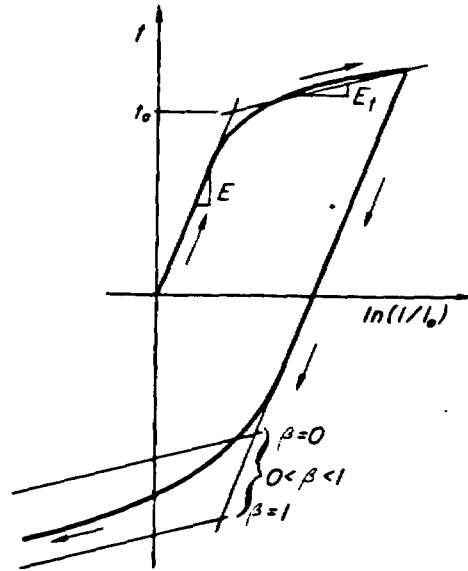


Figure 6. The typical behavior of a ductile metal bar loaded first in uniaxial tension followed by uniaxial compression. The straight line approximation is characterized as an elastic modulus  $E$ , a yield stress  $t_0$ , a strain hardening modulus  $E_t$ , and a hardening parameter  $\beta$  where kinematic hardening is obtained with  $\beta = 0$ , isotropic hardening is obtained with  $\beta = 1$ , and a linear combination of the two is obtained for  $\beta$  between zero and one.

A von Mises yield surface is used with a hardening behavior which is a linear combination of isotropic and kinematic [24]. Isotropic hardening is the behavior where the radius of the yield surface grows equally in all directions due to plastic straining. Kinematic hardening is the behavior where the radius of the yield surface remains constant but the center translates in the direction of the plastic strain rate. When the stress state contacts the yield surface, plastic straining occurs. Thus, the yield condition is given by

$$\phi = 1/2 \xi'_{ij} \xi'^{ij} - k^2 (d^p) = 0 \quad (34)$$

where the prime indicates deviatoric components and  $\xi'_{ij}$  is the back stress defined as

$$\xi'_{ij} = t'_{ij} - \alpha_{ij} \quad (35)$$

The center of the yield surface is given by  $\alpha_{ij}$  which is determined by

$$\nabla_{rs} \alpha_{rs} = \dot{\alpha}_{rs} - g^{rm} w_{mn} \alpha^{ns} - g^{sm} w_{mn} \alpha^{nr} = (1-\beta) \frac{2}{3} H d_{rs}^p \quad (36)$$

The plastic hardening modulus  $H$  is computed from the elastic modulus  $E$  and the tangent modulus  $E_t$  as

$$H = \frac{EE_t}{E - E_t} \quad (37)$$

The amount of hardening which is kinematic is given by  $(1-\beta)$ . The radius  $k$  of the yield surface which grows due to isotropic hardening is given by

$$\sqrt{2} \dot{k} = \beta \frac{2}{3} H |d_{rs}^p| \quad (38)$$

or upon integration

$$\sqrt{2} k = \sqrt{(2/3)} t_0 + \beta \frac{2}{3} H \int_0^t |d_{rs}^p| dt \quad (39)$$

The amount of hardening which is isotropic is given by  $\beta$ . An associated flow rule is used so that the plastic strain rate is normal to the yield surface.

$$d_{rs}^p = \lambda \frac{\partial \phi}{\partial t'_{rs}} = \lambda \xi'_{rs} \quad (40)$$

The magnitude of the plastic strain rate is given by

$$|d_{rs}^p| = \lambda (\xi'_{rs} \xi'^{rs})^{1/2} = \lambda \sqrt{2} k \quad (41)$$

At yield,  $\dot{\phi} = 0$ ,

$$\dot{\phi} = \xi'_{rs} (\dot{\gamma}'^{rs} - \dot{\alpha}'^{rs}) - \sqrt{2} k (\sqrt{2} \dot{k}) = 0 \quad (42)$$

The stress rate is related to the elastic strain rate, through the relation

$$\dot{\gamma}^{rs} = C^{rsmn} (d_{mn} - \lambda \xi'_{mn}) \quad (43)$$

Equations (40) and (41) are substituted into Equations (36) and (38), respectively, and these, together with Equation (43) are substituted into Equation (42). The resulting expression is simplified using Equation (34) and the proportionality rate is obtained as

$$\lambda = \frac{\xi'_{rs} C^{rsmn} d_{mn}}{\xi'_{rs} C^{rsmn} \xi'_{mn} + \frac{4k^2 H}{3}} \quad (44)$$

Thus, the stress rate during yielding is given by

$$\dot{\gamma}^{rs} = (C^{rsmn} - \bar{C}^{rsmn}) d_{mn} \quad (45)$$

where by comparison of Equations (43) and (45) and using Equation (44) there results:

$$\bar{C}^{rsmn} = \frac{C^{rs1j} \xi'_{ij} \xi'_{pq} C^{pqmn}}{\xi'_{ij} C^{1jppq} \xi'_{pq} + \frac{4k^2 H}{3}} \quad (46)$$

The system of Equations (38) through (46) is integrated in time to describe plastic behavior. The details of this numerical integration are covered next.

The main numerical approximation underlying the incremental relations, as in all the constitutive subroutines, is that the strain rate is constant during the time step from  $n$  to  $n + 1$ . The method used for integrating the elastic-plastic calculations is reported by Krieg and Key [8, 9]. The method may be considered that of stepping out elastically in deviatoric stress space and, if the resulting "trial state" is beyond the yield surface, then the stress is scaled back radially to the updated von Mises yield surface. The size of the updated yield surface is found from Equation (39) and the position from an Euler integration of Equation (36). In this manner, the updating of stress and the yield surface position and size are found simultaneously. The method applies equally well regardless of the initial position of the stress state. While a conceptually "simplistic" process, it is an excellent numerical approximation for integrating the conventional isotropic-kinematic hardening von Mises plasticity with an associated flow rule. The accuracy has been compared by Krieg and Krieg [10] to other methods for the case of no hardening.

This explanation is made more concrete by using the mathematical equations which follow. The stress  $t^n$ , position of the center of the yield surface  $\alpha^n$ , and effective plastic strain  $e_p^n$ , all at time  $n$ , and the strain rate  $d^{n+1/2}$  at time  $n + 1/2$  are taken to be known. The steps taken are then:

- (1) The radius of the yield surface is calculated.

$$\sqrt{2} k = \sqrt{2/3} t_y + \rho \frac{2H e^n}{3}$$

- (2) The elastic "trial" stress state, for the end of the increment is calculated.

$$\sigma_{ij}^T = t_{ij}^n + C_{ijmn}^{mn} \frac{n+0.5 \Delta t}{2}$$

- (3) The vector magnitude of the deviatoric effective trial stress is calculated,

$$\xi_{ij}^T = \sigma_{ij}^T - \alpha_{ij}^n \text{ Deviator,}$$

and compared to the radius of the yield surface.

$$\phi = |\xi_{ij}^T| - 2k$$

- (4) The incremental process is elastic if  $\phi \leq 0$  and the final stress is the trial stress.

$$t_{ij}^{n+1} = \sigma_{ij}^T$$

The incremental process is at least partially plastic if  $\phi > 0$  and the remaining step (5) must be followed.

- (5) Updated values of the yield surface position and size (indirectly as the effective plastic strain) are calculated and the trial stress is scaled back to this surface to give the final stress.

$$C_5 = \frac{1 - \frac{\sqrt{2} k}{|\xi_{ij}^T|}}{1 + (H/3\mu)}$$

$$e_p^{n+1} = e_p^n + C_5 |\xi_{ij}^T| / \sqrt{6\mu}$$

$$\alpha_{ij}^{n+1} = \alpha_{ij}^n + (1 - \beta) \frac{C_5 H}{3\mu} \xi_{ij}^T$$

$$t_{ij}^{n+1} = t_{ij}^n - C_5 \xi_{ij}^T$$

As stated in a previous section, this stress state is then rotated a half step. It should be mentioned that the back stress  $\alpha_{ij}$  must also be rotated in the same way as the stress.

### 3.3 Volumetric Plasticity

Rocks, foams, and other void containing materials exhibit a behavior that is pressure dependent. These materials crush or compact under pressure. Their failure in shear can also be sensitive to pressure. We model these characteristics using a pressure dependent isotropic plasticity theory. The yield surface in principal stress space is a surface of revolution with its axis centered about the hydrostat and the open end pointing into the compression direction. The open end is capped with a plane which is at right angles to the hydrostat. The deviatoric part is elastic-perfectly plastic so the surface of revolution is stationary in stress space. Neither isotropic nor kinematic hardening is allowed in the deviatoric directions. The volumetric part however has variable strain

hardening so the end plane moves outward during volumetric yielding. The volumetric hardening is defined by a set of pressure-volumetric strain relations. A flow rule is used such that deviatoric strains produce no volume change.

The theory is most easily discussed by separating the problem into volumetric and deviatoric parts. The strain rate is decomposed into the respective parts by

$$\dot{\gamma} = d_k^k \quad (47)$$

$$d'_{rs} = d_{rs} - \frac{1}{3}\gamma g_{rs},$$

and the stress is separated into the respective parts by

$$p = -\frac{1}{3}t_k^k \quad (48)$$

and

$$t'_{rs} = t_{rs} + pg_{rs}$$

The yield function is defined as the product of two functions,  $\phi_s$  describing the surface of revolution, and  $\phi_p$  describing the plane which is normal to the pressure axis. These are given by:

$$\phi_s = \frac{1}{2}t'_{rs}t'^{rs} - (a_0 + a_1p + a_2p^2) \quad (49)$$

$$\phi_p = p - f(\gamma).$$

The volumetric hardening is given by  $f(\gamma)$ .

Let us consider the volumetric part first. The pressure is calculated as:

$$p = \begin{cases} f(\gamma) & \text{for } \phi_p \geq 0, \dot{\gamma} \leq 0 \\ p(t_u) - K_0 \int_{t_u}^t \dot{\gamma} dt & \text{for } \phi_p \leq 0, \dot{\gamma} > 0 \end{cases} \quad (50)$$

where  $t_u$  is the most recent time the conditions of Equation (50)<sub>1</sub> were met. Initially,  $t_u$  is zero and  $p(0)$  is zero. The first condition describes plastic loading and the second describes the elastic condition, either in loading or unloading.

The function  $f$  which describes the pressure versus the volume strain behavior during loading is depicted in Figure 7. Unloading from any point results in stress states which lie along the curve with a slope of  $K_0$ .

Tensile fracture has not occurred so long as the pressure does not become so tensile or negative as to have a zero or imaginary deviatoric yield stress. Fracture is not assumed for

$$p > h, \quad (51)$$

where  $h$  is the minimum root of the polynomial  $a_0 + a_1 p + a_2 p^2 = 0$ . If Equation (51) fails to hold, the pressure is set equal to  $h$ .

We now consider the deviatoric component where almost conventional plasticity theory is used. If  $\phi_s < 0$  or  $\phi_s = 0$  and  $\dot{\phi}_s < 0$ , the material is assumed to behave elastically in the deviatoric mode, hence,

$$\tau'_{rs} = 2\mu d'_{rs} \quad (52)$$

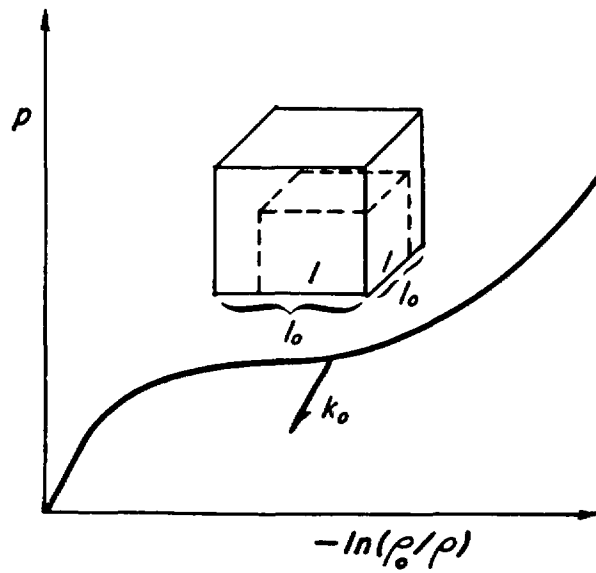


Figure 7. The pressure versus volume strain behavior for a porous material. Unloading is assumed to occur elastically with a modulus of  $K_0$ .

where  $\mu$  is the shear modulus. If, however, the yield surface is reached and the end state is outside the yield surface, i.e., if

$$\phi_s > 0 \quad (53)$$

then part of the time step must have been plastic. In that case, the strain rate is taken as the sum of an elastic part and a plastic part,

$$d_{rs} = d_{rs}^e + d_{rs}^p \quad (54)$$

The plastic strain rate is assumed to lie in a direction normal to the yield surface  $\phi_s$  in the deviatoric subspace of the stress which is written as

$$d_{rs}^p = \lambda \frac{\partial \phi_s}{\partial t} = \lambda t'_{rs} \quad (55)$$

This is a flow rule which results in zero plastic volume strain from deviatoric yielding. The function  $\lambda$  is determined from the loading condition.

$$\dot{\phi}_s = \frac{\partial \phi_s}{\partial t'_{rs}} \dot{\gamma}'_{rs} + \frac{\partial \phi_s}{\partial p} \dot{p} = 0 \quad (56)$$

Expressing the stress rate in terms of the elastic strain rate provides

$$2\mu t'^{rs} (d'_{rs} - \lambda t'_{rs}) - (a_1 + 2a_2 p) \dot{p} = 0 \quad (57)$$

or

$$\lambda = \frac{2\mu t'^{rs} d'_{rs} - (a_1 + 2a_2 p) \dot{p}}{2\mu t'_{rs} t'^{rs}} \quad (58)$$

Thus, the deviatoric stress rate during yielding is given by

$$\dot{\gamma}'_{rs} = 2\mu \left( \delta_r^m \delta_s^n \frac{t'_{rs} t'^{mn}}{t'_{ij} t'^{ij}} \right) d'_{mn} + \frac{t'_{rs} (a_1 + 2a_2 p)}{t'_{ij} t'^{ij}} \dot{p} \quad (59)$$

The second term in Equation (59) accounts for the change in radius of the yield surface as the pressure changes.

This model is implemented numerically in the following manner. The volumetric calculations are carried out first, followed by the deviatoric calculations. At the start of the step the stress at time  $n$  and the strain rate at time  $n+1/2$  are known and the stress at time  $n+1$  is sought. The pressure  $p^{n+1}$ , which is determined first, is used to define the radius of the yield surface. In the deviatoric calculations the entire step from time  $n$  to  $n+1$  is then made using the final radius. The elastic-perfectly plastic deviatoric calculation from time  $n$  to  $n+1$  is carried out in closed form assuming the strain rate is constant during the step. The details of this exact integration are found in Krieg [25]. The steps taken are as follows:

- (1) The pressure  $p$  and the deviatoric stress  $t_{ij}$  at time  $n$  are computed. The volumetric strain rate  $\gamma$  and deviatoric strain rate  $d_{ij}$  at time  $n+1/2$  are computed.
- (2) The volumetric strain at time  $n+1$  is calculated and compared to the past minimum  $\gamma_u$

$$\gamma^{n+1} = \gamma^n + \gamma^{n+1/2} \Delta t_{n+1/2} .$$

If  $\gamma^{n+1} > \gamma_u$ , the step is elastic and

$$p^{n+1} = p^n - K_0 \gamma^{n+1/2} \Delta t_{n+1/2} .$$

If  $\gamma^{n+1} \leq \gamma_u$ , plastic loading is occurring and

$$p^{n+1} = f(\gamma^{n+1})$$

$$\gamma_u = \gamma^{n+1} .$$

- (3) A check for tensile failure is made. If failure has occurred, the pressure at time  $n+1$  is set equal to  $h$ . The stress state is then at the tip of the surface of revolution and the deviatoric stress must be zero

$$t_{ij}^{n+1} = -p^{n+1} \delta_{ij} = -h \delta_{ij}.$$

If failure has not occurred, the deviatoric stresses are sought.

- (4) The stress  $t^n$  at time  $n$  is scaled back to the yield surface,  $\phi_s = 0$ , if it lies beyond it. A trial stress  $s^{n+1}$  at time  $n+1$  is computed assuming elastic behavior for the increment and evaluated for yielding

$$s^{n+1} = s^n + 2\mu d^{n+1/2} t_{n+1/2}.$$

If  $\phi_s(s^{n+1}, p^{n+1}) \leq 0$ , the process is elastic and  $t^{n+1} = s^{n+1}$ .

- (5) If  $\phi_s(s^{n+1}, p^{n+1}) > 0$ , plasticity is occurring. The point of contact with the yield surface and the remaining increment of strain are computed

$$\phi_s(s^{n+1} + \lambda(s^{n+1} - t^n), p^{n+1}) = 0$$

$$t_c^{n+1} = s^{n+1} + \lambda(s^{n+1} - t^n)$$

$$\epsilon^{n+1/2} = -\lambda d^{n+1/2} \Delta t_{n+1/2}.$$

- (6) An exact integration of the plasticity equations is carried out for the remaining strain increment to find  $t^{n+1}$ .

The rotation of the stress state over a half time is carried out as described in an earlier section.

### 3.4 Metallic Creep

If a ductile polycrystalline material is at a temperature greater than roughly one-third the melting temperature, the material will undergo time dependent shear deformation under an imposed shear stress. The volumetric behavior is assumed to be linearly elastic so that a decomposition can be made into volumetric and deviatoric parts. The strain rate (stretching tensor) is decomposed as follows.

$$\dot{\gamma} = d_k^k \quad (60)$$

$$d'_{rs} = d_{rs} - \frac{1}{3}\dot{\gamma}\delta_{rs} \quad (61)$$

and the stress is separated in a similar manner as

$$p = -\frac{1}{3}t_k^k \quad (62)$$

$$t'_{rs} = t_{rs} + p\delta_{rs} \quad (63)$$

The rate of change of the pressure is then found as

$$\dot{p} = -K\dot{\gamma} \quad (64)$$

where K is the elastic bulk modulus.

The deviatoric strain rate is decomposed into elastic and creep parts as

$$d'_{rs} = (d'_{rs})_e + (d'_{rs})_c \quad (65)$$

and the elastic term stated in terms of the stress flux.

$$t'_{rs} = 2\mu(d'_{rs})_e \quad (66)$$

The creep strain rate is taken in a conventional manner to be in the direction of the deviatoric stress and to be described by power law creep.

$$(d'_{rs})_c = \bar{A}(\theta) |t'_{ij}|^m t'_{rs} \quad (67)$$

The function,  $A(\theta)$ , is taken to be of the form  $A \exp(Q/R\theta)$  where  $Q$  is the activation energy,  $R$  is the universal gas constant, and  $\theta$  is the temperature. Equations (65) - (67) are combined to give the result:

$$\bar{\gamma}'_{rs} = 2\mu(d'_{rs} - \bar{A}(\theta) |t'_{ij}|^m t'_{rs}) \quad (68)$$

The deviatoric stress flux and the pressure rate are integrated separately in time and combined to give the total stress.

The numerical implementation of the creep equation is more involved than most constitutive equations because of severe accuracy problems caused by the stress exponent. The method used in SANCHO follows that of Krieg [26]. A summary of the method follows.

The decomposition of the strainrate (stretching tensor) and stress tensor into volumetric and deviatoric parts is made initially. The calculation of the pressure at time step  $n$  is updated in the following manner.

$$p^n = p^{n-1} - \frac{1}{3} K \bar{\gamma}^{n-1/2} \Delta t \quad (69)$$

The deviatoric stress flux integration is much more involved. The differential equation for the flux is very simply stated at time step  $n-1/2$  as:

$$(\bar{\gamma}'_{rs})^{n-1/2} = 2\mu(d'_{rs} - \bar{A}(\theta) |t'_{ij}|^m t'_{rs})^{n-1/2} \quad (70)$$

where the elastic shear modulus,  $\mu$ , creep constant,  $m$ , and temperature function,  $\bar{A}(\theta)$ , as well as the strainrate  $(d'_{rs})^{n-1/2}$  are approximated as constant over the time interval  $\Delta t$ .

The numerical integration of Equation (70) is not simple since the equation is very non-linear, containing the norm of a tensor which is furthermore raised to a power. It also is difficult to integrate analytically for the same reason. The approach used is to replace the differential equation with approximate differential equations which can be integrated analytically. The particular approximate differential equation chosen depends upon the location of the stress state in non-dimensional deviatoric stress space. The stresses are non-dimensionalized with respect to the deviatoric stress state which is asymptotically approached at long times. If deviatoric stresses are denoted as  $S_{ij}$ , then

$$(S_{rs})_{\infty} = \frac{|d'_{pm}|^{\frac{1}{m+1}}}{A} \frac{d'_{rs}}{|d'_{ij}|} \quad (71)$$

The first approximate differential equation is given as

$$S_{ij} + \frac{C_3 S_{ij}}{1 + (m-1)C_3 t} = 2\mu d'_{ij} \quad (72)$$

$$\text{where } C_1 = (S_0/S)^{m-1}$$

$$C_2 = S_{\infty} / |d'_{rs}|$$

$$C_3 = 2\mu C_1 / C_2$$

$$S_{\infty} = |(S_{rs})_{\infty}|$$

This equation is obtained by approximating  $|S_{ij}|^{m-1}$  in the original differential equation with the solution for the case of stress relaxation. Equation (72) then applies when the stress state is far from  $(S_{rs})_{\infty}$ . The exact solution to Equation (72) is given as

$$S_{ij} = f c_4 d'_{ij} + \left[ (S_{ij})_0 - c_4 d'_{ij} \right] f^{-\frac{1}{m-1}}$$

$$\text{where } c_4 = \frac{2\mu}{m c_3}$$

$$f = 1 + (m-1) c_3 t$$

The accuracy of this solution is controlled by limiting the time step size to:

$$t \leq \frac{c_2}{2\mu} \left( 0.04 + \frac{0.54}{m} \right)$$

A second approximate differential equation is found by expressing the differential equation in terms of the variable:

$$X_{ij} = S_{ij} - (S_{ij})_{\infty}$$

An approximate differential equation is then:

$$\frac{\partial X_{ij}}{\partial t} = \frac{-2\mu |d'_{rs}|}{S_{\infty}} \left[ X_{ij} + (m-1) Z (S_{ij})_{\infty} / S_{\infty}^2 \right]$$

$$\text{where } Z = X_{ij} (S_{ij})$$

and where higher order terms in  $X_{1j}$  are dropped. The exact solution to this differential equation is

$$S_{1j} = (S_{1j})_{\infty} + g \left[ (S_{1j})_0 - (S_{1j})_{\infty} \right] - \left[ \frac{(S_{rs})_0 (S_{rs})_{\infty}}{S_{\infty}^2} - 1 \right] (g^m - g) (S_{1j})_{\infty}$$

where  $g = \exp(-2\mu t/C_2)$

This solution holds when the deviatoric stress state is near  $(S_{1j})_{\infty}$ . It is used whenever the stress is such that

$$|S_{1j} - (S_{1j})_{\infty}| \leq 0.12 + 0.77/m$$

If this condition holds at the beginning of the time step, then the final stress state will be found with a stress difference less than five percent of the correct answer for  $m \leq 10$ .

The approximate differential equations are good for small time steps but the solution to the first approximate differential equation diverges from the true solution for long time steps. For that reason the application of a particular solution has been limited inside the constitutive subroutine to a time duration such that the error with respect to the true solution is less than 5%. If that time is less than the specified time increment, then the integration procedure is reapplied for the remainder of the time increment. The second subincrement of time may involve the same approximate differential equation or the other one. This automatic error control procedure may require up to seven subincrements in an extreme case.

The final deviatoric stress is then combined with the pressure from Equation (74) to produce the final stress state.

### 3.5 Material State Parameter

The material state parameter may be used to determine more about the behavior of the non-linear material models. To characterize the state of each element as the calculations proceed in addition to the stress or other state variables, the material state parameter may be included in the printed output. The meaning of this parameter varies from stress relation to stress relation. The finite strain plasticity relation calculates the ratio of the trial elastic stress to the current yield stress. Thus, if the parameter has a value of 1.2 at a particular time step, the magnitude of the trial elastic deviatoric stress was 20% greater than that required to cause yielding. The volumetric plasticity material provides the same state parameter as the plasticity relation except that, if a tensile failure has occurred, the state parameter will be -1.

### 3.6 Finite Strain Mechanical Properties

The finite strain relations do require some care in specifying the required constants. Because these relations involve a very specific stress and strain, the data from which the constants are obtained must be plotted in terms of these variables. The uniaxial tension-compression test used in determining the constants for the elastic-plastic parameters is a good example. Figure 8(a) shows the gage section of a bar in such a test. An axial force  $F$  is applied to the bar in Figure 8(b) which causes it to elongate. At the same time that it elongates the cross-sectional area becomes smaller. Figure 8(c) shows a typical measured result from a test of this type. The horizontal axis corresponds to the infinitesimal strain measure. It is referred to as engineering strain and it is the output which strain gages are designed to provide. These measurements need to be expressed in terms of the Cauchy stress versus logarithmic strain for proper inclusion in the models used here.

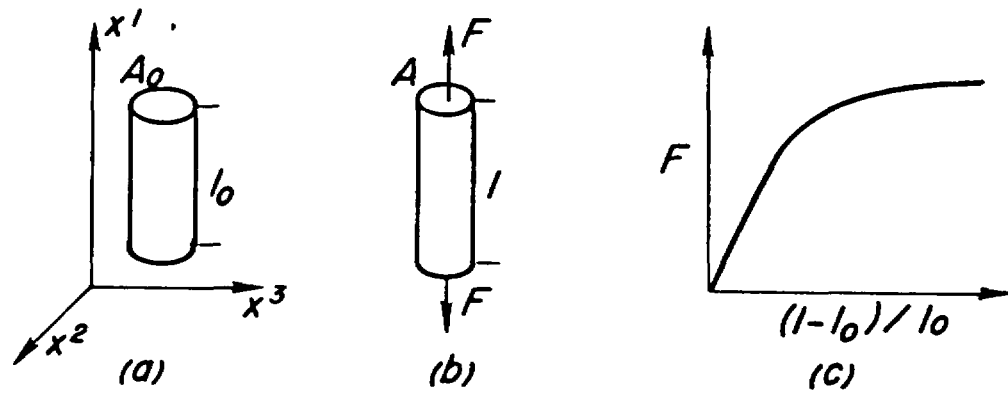


Figure 8. The standard uniaxial tension test.

Using  $r$  for the radius of the test specimen, the deformation gradient is given by

$$[F_{\alpha}^k] = \begin{bmatrix} \frac{l}{l_0} & 0 & 0 \\ 0 & \frac{r}{r_0} & 0 \\ 0 & 0 & \frac{r}{r_0} \end{bmatrix}$$

It is assumed that the deformation is homogeneous. The one nonzero component of the Cauchy stress is  $t^{11}$  and is given by  $F/A$ . The integral of the stretching in the  $x^1$  direction  $\int_0^t d_{11} dt$  is the logarithmic strain  $\ln(l/l_0)$ . Thus, the measurements presented in Figure 8(c) must be replotted in

the form shown in Figure 9 before the constants of the stress relation are determined. Should necking occur in the gage section, its effects must be eliminated from the data.

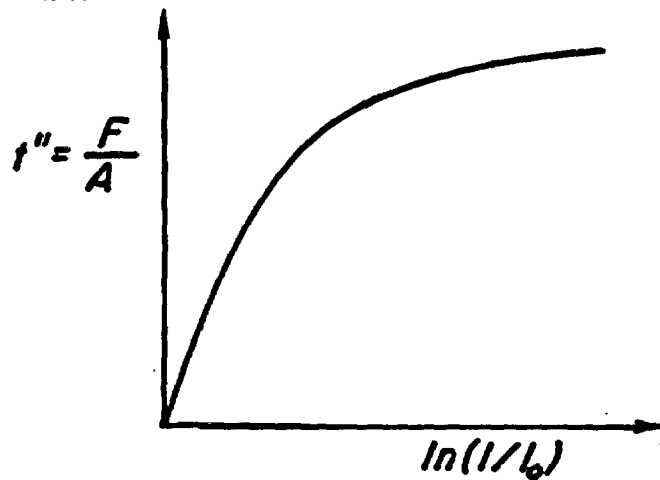


Figure 9. The results of the standard uniaxial tension test expressed in terms of the Cauchy stress versus the logarithmic strain.

The bulk properties required by the volumetric plasticity relation present another situation where the data must be replotted before the constants can be determined for the finite strain case. Figure 10(a) shows a cube of material before being loaded. A pressure  $p$  is applied as shown in Figure 10(b) which causes it to compress. Figure 10(c) shows a typical measured result from a test of this type. Again, these measurements need to be expressed in terms of the Cauchy pressure versus the logarithmic bulk strain.

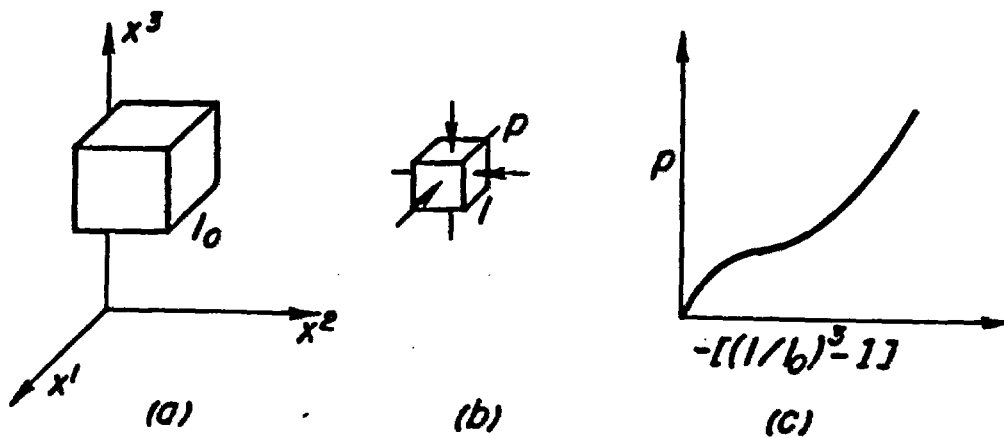


Figure 10. The standard hydrostatic compression test.

Assuming that the deformation is homogeneous, the deformation gradient is given by

$$[F_{\alpha}^k] = \begin{bmatrix} \frac{l}{l_0} & 0 & 0 \\ 0 & \frac{l}{l_0} & 0 \\ 0 & 0 & \frac{l}{l_0} \end{bmatrix}$$

The Cauchy stress is given by  $t^{kn} = -p g^{kn}$ . Using Euler's equation of continuity the integral of the spherical portion of the stretching  $\int_0^t \frac{d_k}{k} dt$  is the logarithmic bulk strain,  $\ln(\rho_0/\rho)$ . Thus, the data presented in Figure 10(c) must be replotted in the form shown in Figure 11 before the constants for the stress relation are determined.

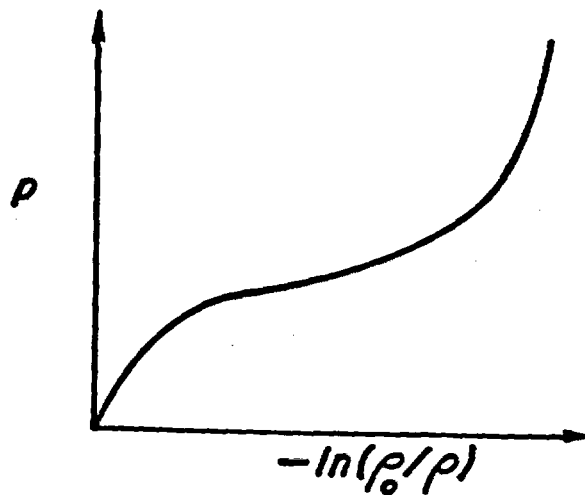


Figure 11. The results of the standard hydrostatic compression test expressed in terms of the Cauchy pressure versus the logarithmic bulk strain.

#### 4 SANCHO USER INSTRUCTIONS

The input to SANCHO is coded to accept keyword input using a free-field reader. This makes the code more user friendly for data construction, particularly in an interactive mode. The free-field reader allows either alphanumeric, integer or floating point numbers to be used interchangeably. The free-field reader used in SANCHO uses only commas as field delimiters. Embedded blanks in alphanumeric variables are retained while blanks in other variables are ignored. Alphanumeric keywords are limited to a maximum of 10 characters. All non-alphanumeric fields are initialized to 0, so that if a given quantity is 0, or does not need to be entered, then a series of commas suffice to skip fields, e.g., 1,4,,3 will be read as 1, 4, 0, 3. Fields may be left blank if no further entry is needed. The \* character may be used to continue a field onto a second data card. The continuation takes the form ...,\* where the \* becomes an entry in the last field and tells the free-field reader to begin reading the next input card. The \$ character may be used to end a data card and the remaining columns on the card used for user comments.

SANCHO does not contain a mesh generator and therefore relies upon externally generated nodal and element data. SANCHO currently accepts mesh input generated by the QMESH [3] mesh generator. QMESH provides nodal coordinate data, element connectivity, and boundary flag identifiers for use in computing element stiffnesses, for applied loads and for assigning boundary conditions. Any other mesh generator that employs the concept of boundary flags could be adapted for use with SANCHO.

SANCHO can be used to perform thermal stress calculations using thermal data supplied by an independent heat conduction code that writes a temperature tape in the proper format. SANCHO will linearly interpolate between times on the thermal tape to obtain temperatures at the current time step. The format of the temperature tape is provided in a later section.

The input is divided into three distinct sections to simplify the task of preparing code input. Within limits, each section is order independent with regard to input, however, the problem definition section and the

material property section must be ended with an 'ENDSET' command card and the first card in the data must be a TITLE card. The last card in the boundary condition and loads specification section, which is the last card in the input, must be an 'END' card. The first section of input is used to define the class of problem being solved. Information such as type of problem or size of time step is input here. The second section is devoted to the description of the materials being used in the problem. The third and final section provides all the data necessary to define loads, boundary conditions, slidelines, etc. These input groups will be described in the following sections.

In order to simplify the discussion of the necessary input, certain conventions will be adopted. Most data cards will begin with a keyword followed by any required data. All alphanumeric input will be capitalized. The symbols [ ] will enclose all non-keyword data. All program default values will be enclosed in { }. The input cards will be discussed in alphabetical order of keywords with a few exceptions. The section one input is given below.

#### 4.1 Problem Definition - Section One Input

##### TITLE

There is no keyword associated with this card. The user is allowed 60 columns to input a title associated with the particular run. The TITLE card must be present and must be the first card in the input stream.

##### AXISYM

This card requests that an axisymmetric analysis is to be performed. {AXISYM}.

CONTROL.[nummat,numlp,numdt,klin]

This card is necessary to establish the problem size for setting up the storage arrays.

nummat- The number of materials in the problem {1}  
numlp- The number of pressure-time points input {0}  
numdt- The number of displacement-time points input {0}  
klin- The type of stress measure to be written to tape {3}

Note: KLIN = 1 Cauchy stress and Signorini strain  
= 2 2nd Piola-Kirchoff stress and Green-St.Venant strain  
= 3 Cauchy stress and Signorini strain where the bulk strain equals the  $\ln(\rho_0/\rho)$ .

DEBUG

This card requests that debug information be written to the output file and to the plot file. The frequency of this information is specified by the ntout parameter on the SOLUTION card described below. This option can be used by an analyst to produce plots of displacements at iterations rather than at converged solutions. WARNING: Use of this option can result in large output plot files. The user is encouraged to limit the numbers of iterations by setting a low value of meq on the SOLUTION card.

DXSCALE.[dtx]

This card lets the user control the stability of the central difference time integrator by multiplying the internally computed time step by a factor, dtx. Some problems may show a local instability which may be removed by reducing the critical time step. {0.9}

dtx- Multiplier of the internally computed critical time step to insure stability. For most calculations the default value should be used.

ELEMENTS.[e11.e12.e13.e14.....eln]

This card selects the elements to be written to the print file. Up to sixteen (16) elements may be requested. If all elements are to be printed only the keyword is required. If no elements are to be printed omit this card.

e11- The number of the element to be printed at the requested time step.

ENDSET

This card is required to end all Section One input.

ISTRESS.[NWORD.sigr.sigz.sigt]

This card is used if a nonzero initial stress state is to be specified.

NWORD- Either the word CONSTANT or VARIABLE is entered to signify whether initial stress state is to be a constant or variable with respect to position. If VARIABLE is specified, then a user supplied subroutine INITST is required to specify the initial stress variation. If CONSTANT is entered, then the following stress values are required and used for all elements.

sigr- Magnitude of constant sigr stress to be applied to every element. {0.0}

sigz- Magnitude of constant sigz stress to be applied to every element. {0.0}

sigt- Magnitude of constant sigt stress to be applied to every element. {0.0}

NODES. [node1,node2,node3,....,node16]

This card is used to define those nodes whose deformations and temperatures are to be printed.

node1- The number of the node whose values are to be written to the print file. Up to sixteen (16) nodes may be specified on this card. If all nodes are to be printed, leave the card blank. If no nodes are to be printed omit this card.

PLANE

This card specifies that a plane strain problem will be solved.  
{AXISYM}

PLOT. [ELEMENT]. [STRESS, STRAIN, STATE]

PLOT. [NODAL]. [DISP, TEMP, RESIDUAL]

PLOT. [GLOBAL]. [RMAG, ITER]

This card(s) selects the quantities written to the post-processing file.

ELEMENT- User selected element quantities will be output.

<STRESS, STRAIN, STATE>

NODAL- User selected nodal quantities will be output.

<DISP, TEMP, RESIDUAL>

GLOBAL- User selected global quantities will be output.

<RMAG, ITER>

If these quantities are omitted no plot data will be written. The individual quantities must be specifically selected. Data is written to FILE11. FILE11 is written in the SEACO [29] format. This card must be used carefully to avoid large output plot files.

## PRINT

Causes the node and element data to be printed. This includes node coordinates, element connectivity and material assignments. Default is no data printed.

## RESTART. [nfreq, nstart]

Allows the user to stop an analysis, check the results, and then restart the analysis from the intermediate stopping point. All previous input cards are necessary on the restart and any card may be changed.

**nfreq-** Specifies the frequency of writing the restart tape. This tape contains multistep restart information so that a successful restart may be done at any previously written time step. Restart data is written to FILE18. {0}

**nstart-** Specifies the time step that should be used for the restart. The job will begin at step nstart and a new restart can be written every nfreq steps. Restart data is read from FILE19. {0}

## SOLUTION. [toler, ntout, meq, toler2]

Parameters controlling iteration and convergence are input on this card.

**toler-** Specifies the percentage of imbalance allowed by the code before convergence is achieved. Imbalance is measured by the L2-norm of the residual forces divided by the L2-norm of the applied loads. {0.5}

**ntout-** Specifies the frequency of intermediate solution information during the iteration process. Such quantities as time, time step, relaxation factor, L2-norm of the applied loads, and percent

imbalance are printed. If this field is left blank, then the information will be printed each iteration. {1}

WARNING: Printing this information for each iteration may lead to an excessive amount of unwanted output.

meq- This is the maximum number of iterations allowed for a given load or time step. If this is reached, the problem will terminate unless 'toler2' is loosely specified. {2000}

toler2- A user defined tolerance which the analyst can employ to modify the convergence specified in 'toler' above. If the problem iterates meq times then the imbalance is checked against toler2 before the analysis is stopped. {toler}

#### THERMAL.thforc

This card sets a flag for a thermal stress analysis. This card is required if a thermal stress analysis is to be performed. Default is no thermal analysis. Thermal input is supplied on FILE56.

thforc- User defined magnitude for thermal force norm. This quantity can be used to override the computed thermal force norm. This may be desirable if the automatically computed norm is too large and the usual tolerance values may be too loose. {0.}

#### TIMEPLOT.[t1.incl.t2.inc2.t3....]

This card is necessary if plot output is desired. The frequency of writing the plot files is controlled by this card. Ten plot increments are allowed. {0.}

t1- Time at which plot output is to start

incl- Time increment for writing of plot output file

t2- Time at which plot output ends for n1 and begins for n2

TIMEPRNT.[t1.incl.t2.inc2.t3.inc3....]

This card is necessary if printed output is desired. The frequency of writing the print files is controlled by this card. Ten print increments are allowed. {0.}

- t1- Time at which printed output will start
- incl- Time increment for writing of output file
- t2- Time at which printed output ends for n1 and begins for n2

TIMESTEP.[t1.n1.t2.n2.t3.n3.t4....]

This card is necessary for the control of the solution steps. RESTART times do not have to correspond to t1. The restart time must however be found within the time frame defined on this card. Ten timestep specifications are allowed.

- t1- Time at which the problem will begin
- n1- Number of timesteps to be taken between t1 and t2
- t2- Final time for this control segment and beginning time for n2

## 4.2 Material Property Specification - Section Two Input

All materials have the following sequence of three input card sets:

### 1. MATERIAL [mtype.ro.gravx.gravy.omega]

This card defines the material type and body force parameters.

mtype- The material type number

ro- Mass density of the material. This is used for the acceleration loading.

gravx- Acceleration in the x-direction{0.}

gravy- Acceleration in the y-direction{0.}

omega- Angular velocity about the y-axis{0.}

Gravx, gravy, and omega need to be input with only one material. Whenever these three values are also read on a later material card, the later values will be the values used in the problem.

### 2. MATERIAL TITLE CARD

The second card for each material is the title that describes this material. There are 80 columns available for the material title.

3. The third card set contains material constants required for each material model. No keyword is used for the third card set. The form of the input for each material model is given on the following pages.

For problems in which several materials are used, the material property sets must be input in the order in which the materials are defined during mesh generation.

ENDSET

Required to end material property section.

MATERIAL TYPE 1 - FINITE STRAIN ELASTIC-PLASTIC STRAIN HARDENING

MATERIAL, 1, ro, gravx, gravy, omega CARD 1

MATERIAL TITLE CARD CARD 2

E,  $\nu$ ,  $t_0$ ,  $E_t$ ,  $\beta$  CARD 3

E- Young's Modulus

$\nu$ - Poisson's ratio

$t_0$ - Yield stress

$E_t$ - Hardening modulus

$\beta$ - Hardening parameter

$\beta=0$  Kinematic

$\beta=1$  Isotropic

Note: If the yield stress  $t_0$  is zero, elastic behavior is assumed.

The following data are required for thermal stress problems. Up to seven pairs of data may be input. If a non-thermal problem is required omit the following cards.

nt, temp1, temp2, temp3, temp4, temp5, temp6, temp7 CARD 4

nt- Number of temperature pairs to be input  $2 < nt < 7$

temp1- Temperature 1

temp2- Temperature 2

.

.

temp7- Temperature 7

eps1, eps2, eps3, eps4, eps5, eps6, eps7 CARD 5

eps1- Thermal strain for temp1

eps2- Thermal strain for temp2

.

.

eps7- Thermal strain for temp7

MATERIAL TYPE 2 - FINITE STRAIN SOIL AND CRUSHABLE FOAM

MATERIAL,2,ro,gravx,gravy,omega

CARD 1

MATERIAL TITLE CARD

CARD 2

$\mu, K_0, a_0, a_1, a_2$

CARD 3

- $\mu$  - Shear modulus
- $K_0$  - Bulk unloading modulus
- $a_0$  - Yield function constant
- $a_1$  - Yield function constant
- $a_2$  - Yield function constant

The following data are input in pairs until up to six pairs have been read. When more than one card is needed, a continuation card is indicated with a \* after the last data on that card.

Pressure-Volume Strain Data

ln.p,ln.p,ln.p,ln.p,\*  
ln.p,ln.p

CARD 4

ln- Volumetric strain ( $\ln \rho/\rho_0$ )

p- Pressure

The following data are required for thermal stress problems. Up to seven pairs of data may be input. If a non-thermal problem is required omit the following cards.

nt,temp1,temp2,temp3,temp4,temp5,temp6,temp7

CARD 5

nt- Number of temperature pairs to be input       $2 < nt < 7$

temp1- Temperature 1

temp2- Temperature 2

.

.

.

temp7- Temperature 7

eps1,eps2,eps3,eps4,eps5,eps6,eps7

CARD 6

eps1- Thermal strain for temp1

eps2- Thermal strain for temp2

.

.

.

eps7- Thermal strain for temp7

**MATERIAL TYPE 3 - POWER HARDENING STEADY STATE CREEP MODEL- ELASTIC BULK**

MATERIAL, 3, ro, gravx, gravy, omega CARD 1  
MATERIAL TITLE CARD CARD 2  
2 $\mu$ , K, A, m, C1 CARD 3

- 2 $\mu$ - Shear modulus
- K- Bulk modulus
- A- Material constant
- m- Stress power constant
- C1- Exponential constant( Q/R $\theta$  if isothermal or Q/R if thermal)

Where Q is the activation energy, R is the universal gas constant, and  $\theta$  is the absolute temperature for the isothermal calculation. If the calculation is not isothermal then the program furnishes the correct temperature for use in the material model.

The following data are required for thermal stress problems. Up to seven pairs of data may be input.

nt, temp1, temp2, temp3, temp4, temp5, temp6, temp7 CARD 4

nt- Number of temperature pairs to be input 2 < nt < 7  
temp1- Temperature 1  
temp2- Temperature 2  
.  
.  
temp7- Temperature 7

eps1, eps2, eps3, eps4, eps5, eps6, eps7 CARD 5

eps1- Thermal strain for temp1  
eps2- Thermal strain for temp2  
.  
.  
eps7- Thermal strain for temp7

### 4.3 Boundary Condition Specification

In SANCHO, multiple boundary condition histories are handled with a single history card and the concept of delay time. Delay time allows a user to specify multiple pressure or displacement histories and relate each one to a specific boundary condition. History specification can be done on a single PHISTORY or a single DHISTORY command. Consider the example shown in Figure 12 where multiple pressure histories are defined using a single PHISTORY card. Each individual history can be uniquely identified by the time associated with the beginning of that history. This time is defined as the "delay time". For use as input into SANCHO, the delay time should be input as a NEGATIVE time.

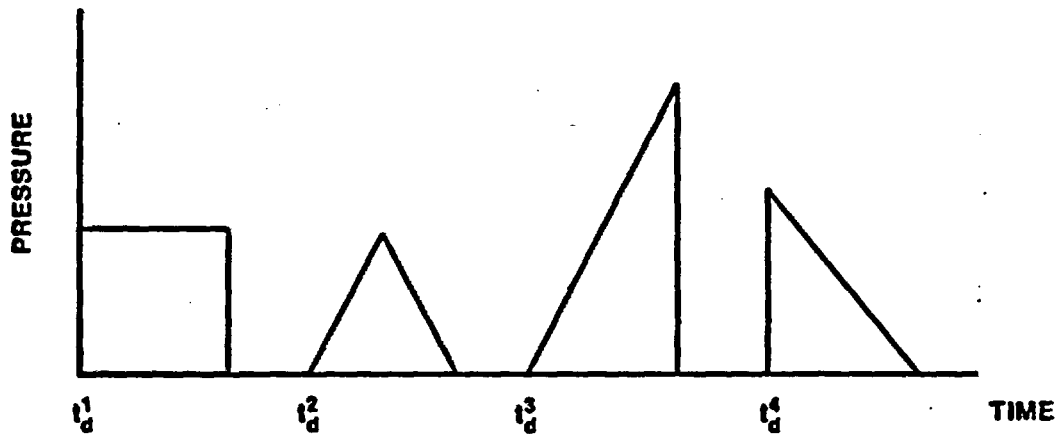


Figure 12. Example of the use of a single PHISTORY card to define multiple time histories through the use of the delay time,  $t_d$ .

DISPR,[b.c. number,value,delay time]

DISPRN,[node number,value,delay time]

These cards specify a radial (R) boundary restraint. DISPR is used with a boundary flag identifier. DISPRN is used to specify a restraint on an individual node.

b.c. number- The unique boundary condition i.d. provided by the mesh generator.  
value- Magnitude of the nonzero specified displacements.  
delay time- Identifier of a particular time history from a DHISTORY card.  
node number- Node number which receives the specified displacement.

DISPZ,[b.c. number,value,delay time]  
DISPZN,[node number,value,delay time]

These cards specify an axial (Z) boundary restraint. DISPZ is used with a boundary flag identifier. DISPZN is used to specify a restraint on an individual node.

b.c. number- The unique boundary condition i.d. provided by the mesh generator.  
value- Magnitude of the nonzero specified displacements.  
delay time- Identifier of a particular time history from a DHISTORY card.  
node number- Node number which receives the specified displacement.

DISPRZ,[b.c. number,value,delay time]  
DISPRZN,[node number,value,delay time]

These cards specify both a radial (R) and an axial (Z) boundary restraint. DISPRZ is used with a boundary flag identifier. DISPRZN is used to specify a restraint on an individual node.

b.c. number- The unique boundary condition i.d. provided by the mesh generator.  
value- Magnitude of the nonzero specified displacements.  
delay time- Identifier of a particular time history from a DHISTORY card.  
node number- Node number which receives the specified displacement.

PRESSURE,[b.c. number,pressure value, delay time]

PRESSURE,[i, j, pi, pj, delay time]

This card allows the specification of an applied pressure on an element face. The two forms of input result from either use of a mesh generator to specify pressure boundary conditions or the use of element I-J side specification.

b.c. number- The unique boundary i.d. provided by the mesh generator.  
pressure value- Constant value of the pressure applied to the element face.  
delay time- Identifier of a particular time history from a PHISTORY card.  
i,j- Identifies the node numbers that define the element face to receive the applied pressure.  
pi,pj- Refers to the pressure values for the respective I and J nodes. A linear pressure variation is allowed along the element face. The program reorders the I-J line definition so that the element lies on the left when going from I to J. Positive pressure acts normal to the element face and in a compressive manner.

SKEW,[b.c. number, angle of skew]

SKEWN,[node number,angle of skew]

This card allows specification of a skewed roller type of boundary condition. The angle of skew is defined, Figure 13, from the positive r-axis to the desired direction of motion along the sliding boundary.

b.c. number- The unique boundary condition i.d. provided by the mesh generator.  
angle of skew- Angle defined from positive r-axis to the desired direction of motion.  
node number- Node number which receives the specified displacement.

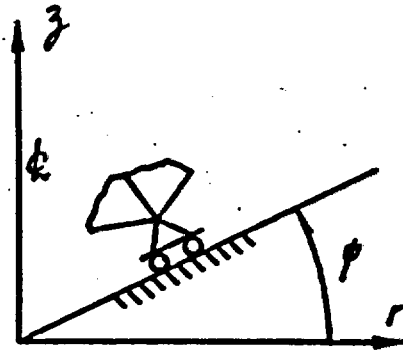


Figure 13. Mixed stress and displacement boundary condition where the node remains free to move in a direction parallel to a line with inclination  $\psi$ .

SLIDE, [master, slave, cf1, cf2, cf3]

This card specifies the master/slave connection for any slidelines in the analysis. A maximum of 12 slidelines is allowed.

- master- Number of the boundary flag i.d. for the slideline master side
- slave- Number of the boundary flag i.d. for the slideline slave side
- cf1- Value of the friction coefficient. if fully fixed use -1.  
Otherwise insert the proper value here. {0.}
- cf2- Value of slideline overlap tolerance to determine when contact of surfaces does occur. {2% of the Master element side length}
- cf3- Value of stress for release of slave node from master surface.  
Value is set to no release, a non-zero value is required to activate this option. {0.}

PHISTORY. [t1.p1.t2.p2.t3.p3.t4.p4....]

This card allows for specification of the time-pressure curve for the analysis. Pressures are always positive acting normal to the element face. Both times and pressures are defaulted to zero.

- t1- Beginning time for the pressure specification
- p1- Pressure value associated with t1
- t<sub>2</sub>- Ending time for the pressure specification

DHISTORY. [t1,d1.t2,d2.t3,d3.t4,d4....]

This card allows for specification of the time-displacement curve for the analysis. Same definition for input as PHISTORY. Both displacements and time values are defaulted to 0.

END

This card is the last line in the SANCHO input stream. The card signifies to terminate the reading of additional input and begin execution.

Table 1. Summary of Keywords and Input

O - Optional Input  
R - Required Input

Problem Definition Section

Keyword	Page
TITLE .....	58
AXISYM .....	58
CONTROL,nummat,numlp,numdt,clin .....	59
DEBUG .....	59
DXSCALE,dtx .....	59
ELEMENTS,e11,e12,e13,....,e16 .....	60
ENDSET .....	60
ISTRESS,NWORD,sigr,sigz,sigt .....	60
NODES,nd1,nd2,nd3,....,nd16 .....	61
PLANE .....	61
PLOT,ELEMENT,STRESS,STRAIN,STATE .....	61
PLOT,GLOBAL,FMAG,ITER .....	61
PLOT,NODAL,DISP,TEMP,RESIDUAL .....	61
PRINT .....	62
RESTART,nfreq,nstart .....	62
SOLUTION,toler,ntout,meq,toler2 .....	62
THERMAL,thforc .....	63
TIMEPLOT,t1,tinc,t2,tinc,t3,....,tn .....	63
TIMEPRNT,t1,tinc,t2,tinc,t3,....,tn .....	64
TIMESTEP,t1,n1,t2,n2,t3,....,tn .....	64

Table 1. Summary of Keywords and Input (Cont.)

Material Property Specification Section

Keyword	Page
ENDSET ..... (R).....	65
<p style="margin-left: 40px;">Material Type 1 - Finite Strain Elastic-Plastic Strain Hardening</p>	
MATERIAL,1,ro,gravx,gravy,omega ..... (O).....	66
material title card	
E,V,to,Et,B	
nt,temp1,temp2,....,tempnt	
eps1,eps2,....,epsnt	
<p style="margin-left: 40px;">Material Type 2 - Finite Strain Volumetric Plasticity</p>	
MATERIAL,2,ro,gravx,gravy,omega ..... (O) .....	67
material title card	
u,k0,a0,a1,a2	
ln,p,ln,p,ln,p,ln,p,ln,p,ln,p	
nt,temp1,temp2,....,tempnt	
eps1,eps2,....,epsnt	
<p style="margin-left: 40px;">Material Type 3 - Power Hardening Steady State Creep</p>	
MATERIAL,3,ro,gravx,gravy,omega ..... (O).....	68
material title card	
2u,K,A,m,c1	
nt,temp1,temp2,....,tempnt	
eps1,eps2,....,epsnt	

Table 1. Summary of Keywords and Input (Cont.)

Boundary Condition Specification (all of these cards are optional)

Keyword	Page
DISPR,b.c. flag number,value,delay time .....	69
DISPRN,node number,value,delay time.....	69
DISPZ,b.c. flag number,value,delay time.....	70
DISPZN,node number,value,delay time.....	70
DISPRZ,b.c. flag number,value,delay time.....	70
DISPRZN,node number,value,delay time.....	70
PRESSURE,b.c. flag number,value,delay time.....	71
PRESSURE,i,j,pi,pj,delay time.....	71
SKEW,b.c. flag number,angle of skew.....	71
SKEWN,node number,angle of skew.....	71
SLIDE,master,slave,cf1,cf2,cf3.....	72
PHISTORY,t1,p1,t2,p2,t3,p3.....	73
DHISTORY,t1,d1,t2,d2,t3,d3.....	73
END.....	73

## 5 EXTERNAL FILE DEFINITION

SANCHO uses several external files for both input and output. These are FILE9 for mesh input, FILE11 for plot output, FILE18 for writing restart output, FILE19 for reading restart information and FILE56 for temperature data. The element plot quantities written to FILE11 post-processing file consist of element, nodal, and global quantities. Element quantities written are divided into stress, strain, and state values. Stress values are the stress measures selected by the user as KLIN on the CONTROL card. These consist of the SIGR, SIGZ, SIGT, and TAURZ values for each element, averaged to the centroid. The strain values are made up of similar quantities. The state values are the quantities stored in the material state array, EPX4. These values include effective plastic strain and physical strain component values. The actual values and their meaning depend on the constitutive model being used.

The nodal values written to the plot file include the two components of displacement, nodal point temperatures, and the nodal components of the residual force vector. The residual force is a measure of the amount of imbalance force at a node. The residual force is decomposed into R-Z components. The global values written to the plot file provide information about the solution behavior. The residual force vector magnitude and the number of iterations for each converged load/time step are the global quantities written. The residual force vector magnitude is defined as the L2-norm of the residual force vector. The list of quantities written to the plot file is given below:

### Nodal Quantities

DISPL R - R or X Displacements  
DISPL Z - Z or Y Displacements  
TEMP - Nodal Temperatures  
RX - Residual Force Component in R or X Direction  
RY - Residual Force Component in Z or Y Direction

### Element Quantities

SIG R - Component of Stress in R or X Direction  
SIG Z - Component of Stress in Z or Y Direction  
SIG T - Component of Stress in Hoop or Planar Direction  
TAU RZ - Component of Shear Stress in RZ or XY Plane  
EPS R - Component of Strain in R or X Direction  
EPS Z - Component of Strain in Z or Y Direction  
EPS T - Component of Strain in Hoop or Planar Direction  
EPS RZ - Component of Shear Strain in RZ or XY Plane  
EPX 1 - State Variable 1  
EPX 2 - State Variable 2  
EPX 3 - State Variable 3  
EPX 4 - State Variable 4  
EPX 5 - State Variable 5

### Global Quantities

ITER - Convergence History  
RMAG - Residual Force Magnitude History

The material models and their use of the EPX4 array for state variable storage is defined below.

### Elastic-Plastic Material Model

EPX 1 -  
EPX 2 -  
EPX 3 - Integral of Plastic Strain  
EPX 4 -  
EPX 5 - Ratio of Trial Stress to Yield Stress

Soil and Crushable Foam Model

Epx 1 -  
Epx 2 -  
Epx 3 -  
Epx 4 -  
Epx 5 - Volumetric Strain

Power Hardening Steady State Creep

Epx 1 -  
Epx 2 -  
Epx 3 - Effective Creep Strain  
Epx 4 -  
Epx 5 -

Temperatures are input into SANCHO through the use of an externally written temperature file, FILE56. The tape is written as an unformatted tape in the following form at the desired thermal time intervals

```
WRITE(56) TIME,(T(I),I=1,NUMNP)
```

where the temperatures, T, are written for each nodal point. SANCHO interpolates linearly between thermal time steps to obtain the thermal solution at the time requested for determination of the structural response.

The user supplied subroutine INITST allows the analyst to apply an initial stress state to the problem. This feature is particularly useful for

geomechanics applications where an overburden stress is a function of depth. The call to subroutine INITST has the following form

```
SUBROUTINE INITST(ZAVG,RAVG,MX,I,BFORCE)
DIMENSION BFORCE(3)
.
.
.
RETURN
END
```

where the calling arguments are defined as:

ZAVG - Z or Y coordinate location of the element centroid  
RAVG - R or X coordinate location of the element centroid  
MX - material number associated with current element  
I - current element number  
BFORCE - values of initial stress will be returned via this argument. three values are required - sigr, sigz, sigt

The call to this subroutine is located within a loop that is executed once per element. A current limitation is that the initial stress be a constant over the element (each of the four integration points has the same initial stress state).

If a user supplied subroutine INITST is required, the execution procedure for a Cray-1 running under COS using the Sandia Engineering Analysis Department procedure file is:

```
ACCESS, DN=$PROC, PDN=PROCS, ID=ACCLIB.
SANCHO, PRO=SUB.
```

Without the user subroutine INITST the execution procedure on the CRAY  
is.

ACCESS, DN=\$PROC, PDN=PROCS, ID=ACCLIB.  
SANCHO.

## 6 EXAMPLE PROBLEMS

Several sample problems are included in this section to demonstrate the input for SANCHO and for code verification purposes. The problems are simple examples that can be compared to a known exact solution or to problems that have been solved by several computer codes. Most of the features in SANCHO will be exercised in these examples. The use of comment cards in the input deck should assist in understanding the input structure.

### 6.1 Free Thermal Expansion

The free thermal expansion of an infinite cylinder was included to demonstrate the input for a thermal stress problem and to demonstrate the ability of SANCHO to solve problems involving thermal loads. The model of the cylinder is shown in Figure 14a with the corresponding temperature and strain data. Poisson's ratio is set to zero to allow only radial motion of the cylinder due to thermal expansion. A single row of ten finite elements evenly spaced through the cylinder thickness was used to represent the cylinder behavior. The convergence tolerance was set to 0.1% which is tighter than usual with SANCHO. This tolerance was chosen because the absence of applied external forces causes the program to compute equivalent thermal loads for use in computing the L2-norm of the applied load vector. For thermal problems, it has been found that this norm is large relative to the typical unbalance force norm and the default convergence tolerance results in an unacceptable solution. The solution improves as the convergence tolerance is reduced. The normal procedure is to use only the user applied external forces, when available, in computing the applied load norm. The radial displacement of the cylinder is compared to the exact solution in Figure 14b at various positions through the thickness for a strain field corresponding to a temperature of 500 degrees.

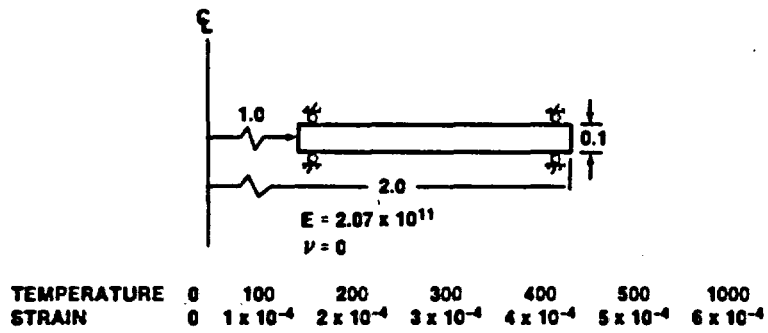


Figure 14a. Geometry and Boundary Conditions for Free Thermal Expansion Problem

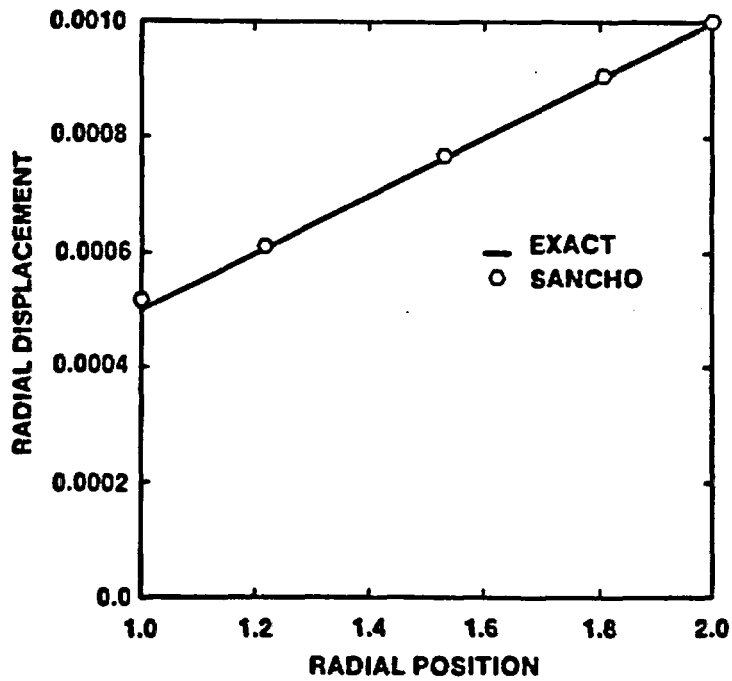


Figure 14b. Comparison of SANCHO Results and Theory for Free Thermal Expansion Example

PROBLEM 1

FREE THERMAL EXPANSION OF A THICK CYLINDER

```
CONTROL,1,3           $ SETS UP STORAGE
SOLUTION,1,5000,5000,.6 $ SETS CONTROL TOLERANCES
Timestep,0,10,1       $ SPECIFIES NUMBER OF TIME STEPS
TIMEPRNT,0,1,1       $ SPECIFIES FREQUENCY OF PRINT
TIMEPLOT,0,1,1       $ SPECIFIES FREQUENCY OF PLOT OUTPUT
THERMAL               $ SPECIFIES A THERMAL STRESS ANALYSIS
NODES                $ ALL NODES WILL BE PRINTED
ELEMENTS             $ ALL ELEMENTS WILL BE PRINTED
PLOT,NODAL,DISP,TEMP,RESIDUAL $ NODAL QUANTITIES WRITTEN TO PLOT FILE
PLOT,GLOBAL,RMAG,ITER $ GLOBAL QUANTITIES WRITTEN TO PLOT FILE
PLOT,ELEMENT,STRESS,STRAIN,STATE $ ELEMENT QUANTITIES WRITTEN TO PLOT FILE
AXISYM              $ DENOTES AXISYMMETRIC ANALYSIS
ENDSET              $ END OF PROBLEM DEFINITION SECTION
MATERIAL,1,1         $ DENOTES MATERIAL - TYPE 1
  * * TEST MATERIAL * *
  2.07E11,0         $ MATERIAL PROPERTIES
  7,0,100,200,300,400,500,1000
  0,1.E-4,2.E-4,3.E-4,4.E-4,5.E-4,6.E-4
ENDSET              $ END OF MATERIAL SECTION
DISPZ,2             $ Z DISPLACEMENT FOR BC CODE 2
END                 $ END OF INPUT DATA
```

## 6.2 Pressurized Infinite Cylinder

The problem of an infinite cylinder loaded into the plastic range by an internal pressure serves as a good check of the elastic-plastic material model. The exact solution can be found in Prager and Hodge [27]. The problem is depicted in Figure 15 with the boundary conditions and material properties given. The analysis was performed by taking 6 steps up to 60% of the maximum pressure and then 20 steps were taken to reach the maximum pressure. A single row of ten finite elements evenly spaced through the thickness were used to model the cylinder. A convergence tolerance of 0.5% was used. The radial displacement of the inner cylinder edge versus  $\rho$ , the radius of the elastic-plastic boundary, is shown in Figure 15a. A value of  $\rho/a = 2$  corresponds to a fully plastic cylinder. For a  $\rho/a = 1.2$ , the radial and hoop stress distributions versus radial position are shown in Figure 15b. The agreement with theory in all cases is excellent.

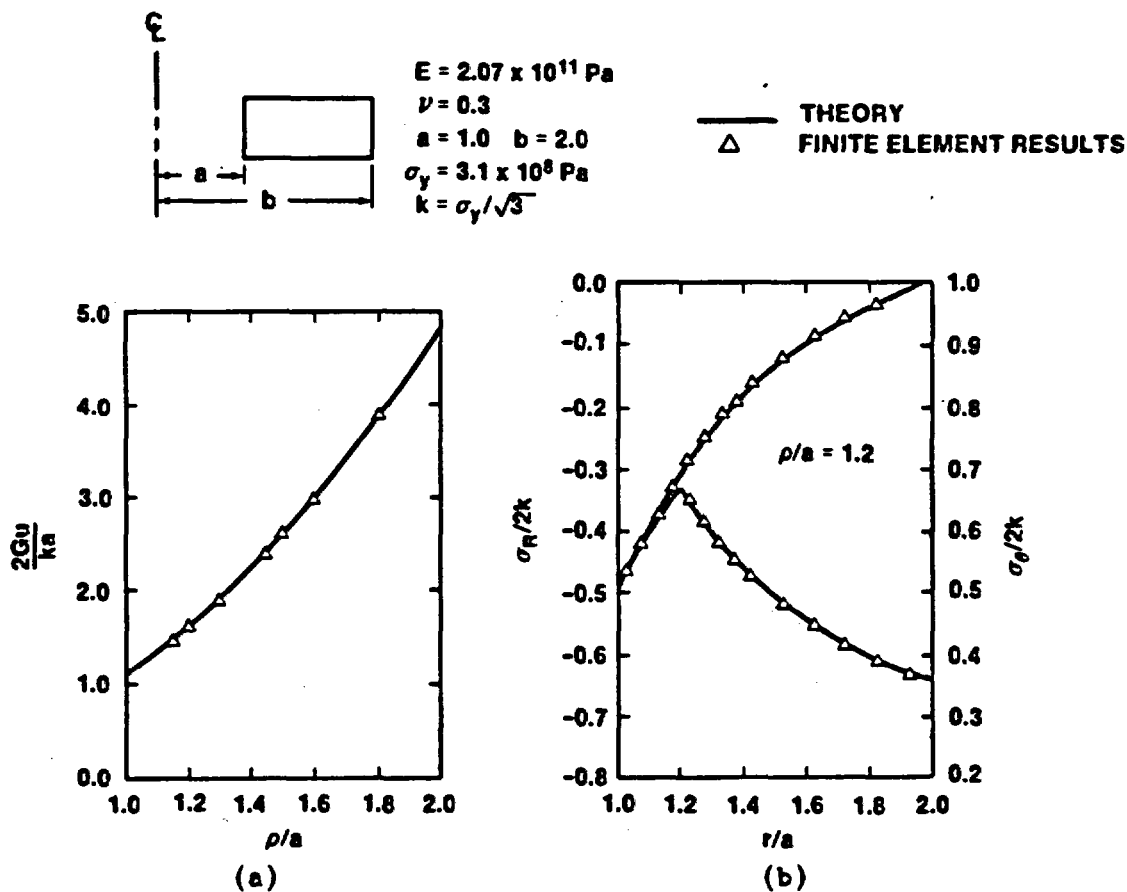


Figure 15. Comparison of SANCHO Results with Theory for an Internally Pressurized Infinite Cylinder.

PROBLEM 2

INFINITE CYLINDER W/ INTERNAL PRESSURE

CONTROL,1,2,0,3	\$ SETS UP STORAGE
SOLUTION,.5,5000,5000,.6	\$ SETS CONVERGENCE AND CONTROL TOLERANCES
TIMESTEP,0.,6.,6,20,1.	\$ SPECIFIES NUMBER OF TIME STEPS
TIMEPRNT,0.,.1,1.	\$ SPECIFIES FREQUENCY OF PRINT
TIMEPLOT,0.,.1,1.	\$ SPECIFIES FREQUENCY OF PLOT OUTPUT
NODES	\$ ALL NODES WILL BE PRINTED
ELEMENTS	\$ ALL ELEMENTS WILL BE PRINTED
PLOT,NODAL,DISP,TEMP,RESIDUAL	\$ NODAL QUANTITIES WRITTEN TO PLOT FILE
PLOT,GLOBAL,FMAG,ITER	\$ GLOBAL QUANTITIES WRITTEN TO PLOT FILE
PLOT,ELEMENT,STRESS,STRAIN,STATE	\$ ELEMENT QUANTITIES WRITTEN TO PLOT FILE
AXISYM	\$ DENOTES AXISYMMETRIC ANALYSIS
ENDSET	\$ END OF PROBLEM DEFINITION SECTION
MATERIAL,1,1.	\$ DENOTES MATERIAL - TYPE 1
* * TEST MATERIAL * *	
2.07E11...3,3.1E8	\$ MATERIAL PROPERTIES
ENDSET	\$ END OF MATERIAL SECTION
PHISTORY,0.,1.,1.,2.	\$ PRESSURE HISTORY PROFILE
DISPZ,2	\$ Z DISPLACEMENT FOR BC CODE 2
PRESSURE,1,.5	\$ PRESSURE SPECIFIED FOR BC CODE 1
END	\$ END OF INPUT DATA

### 6.3 Stress Relaxation

The stress relaxation of a single element is used to demonstrate the accuracy of the elastic creep model. A single finite element is strained using a specified axial displacement. The change in the effective stress as a function of time is compared to the exact solution. The problem is shown in Figure 16a. The top of the element is displaced 0.001m and held constant with time. The effective stress decreases in time as shown by the solid line in Figure 16b. The SANCHO solution took 90 timesteps with a convergence tolerance of 0.1%. The numerical results appear to track the exact solution very well.

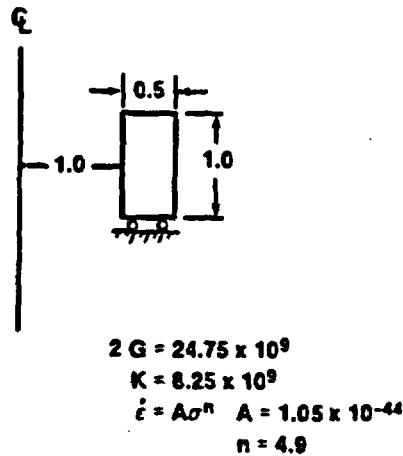


Figure 16a. Model and Boundary Conditions for the Stress Relaxation Example Problem

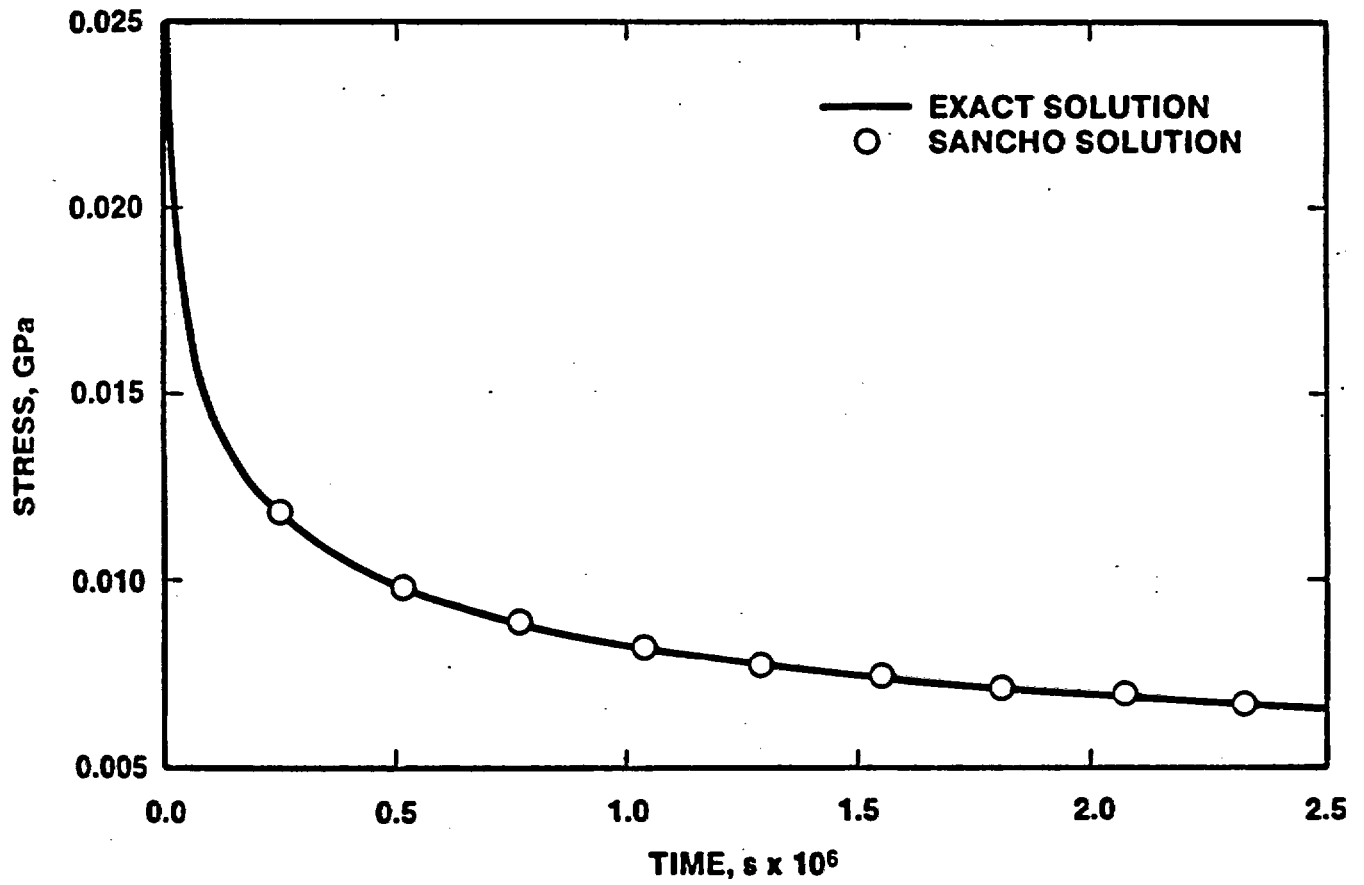


Figure 16b. Stress History for the Relaxation Problem

PROBLEM 3

RELAXATION PROBLEM USING THE CREEP MODEL

CONTROL, 1, .2, 3                   \$ SETS STORAGE REQUIREMENTS  
SOLUTION, .1, 5000, 5000, .1       \$ SETS CONVERGENCE AND CONTROL TOLERANCES  
Timestep, 0, .90, 2.592E6         \$ SPECIFIES NUMBER OF TIME STEPS  
TIMEPRNT, 0, .8, 64E4, 2.592E6   \$ SPECIFIES FREQUENCY OF PRINTED OUTPUT  
TIMEPLOT, 0, .8, 64E4, 2.592E6   \$ SPECIFIES FREQUENCY OF PLOT OUTPUT  
NODES                               \$ ALL NODES WILL BE PRINTED  
ELEMENTS                            \$ ALL ELEMENTS WILL BE PRINTED  
PLOT, NODAL, DISP, TEMP, RESIDUAL  \$ NODAL QUANTITIES WRITTEN TO PLOT FILE  
PLOT, GLOBAL, FMAG, ITER           \$ GLOBAL QUANTITIES WRITTEN TO PLOT FILE  
PLOT, ELEMENT, STRESS, STRAIN, STATE \$ ELEMENT QUANTITIES WRITTEN TO PLOT FILE  
AXISYM                              \$ DENOTES AXISYMMETRIC ANALYSIS  
ENDSET                              \$ ENDS PROBLEM DEFINITION SECTION  
MATERIAL, 3, 2167.                 \$ MATERIAL TYPE 3  
    \* \* TEST MATERIAL \* \*  
24.75E9, 8.25E9, 5.79E-36, 4.9, 20.13 \$ MATERIAL PROPERTIES  
ENDSET                              \$ ENDS MATERIAL SECTION  
DISPZ, 1, .001                     \$ SPECIFIED NONZERO Z DISPLACEMENT BC 1  
DISPZ, 2                            \$ Z DISPLACEMENT FOR BC CODE 2  
DHISTORY, 0, .1, .3, 16E7, 1.     \$ DISPLACEMENT HISTORY FOR BC CODE 1  
END                                 \$ END OF INPUT DATA

#### 6.4 WIPP Benchmark II

The last example problem is much more complex than the preceding examples and therefore relies on comparison with other finite element programs for solution verification. The problem is a complex geotechnical analysis of an underground drift in a multilayered geologic medium, principally rock salt, characterized by creep and with clay seams which are characterized with sliding interfaces with a friction coefficient of zero. Elastic anhydrite and polyhalite layers are also interspersed. The problem was specified as part of the Waste Isolation Pilot Plant (WIPP) Project code comparison activity called Benchmark II [28]. The problem involves determining the response of an infinitely long array of parallel drifts. The problem geometry and boundary conditions are shown in Figure 17. The finite element mesh utilizes 586 elements as shown in Figure 18. The problem requires an initial stress state that varies with depth from the surface. Therefore, the initial stress subroutine INITST is required and is included in the input. The problem allows ten years of creep induced closure which is done in 330 time steps. Many different quantities were compared between the various codes in the referenced study. The vertical closure at the drift centerline as a function of time is shown in Figure 19. The SANCHO solution appears in the center of the solutions reported for this problem. Additional comparisons of stress and slideline response can be found in [28].

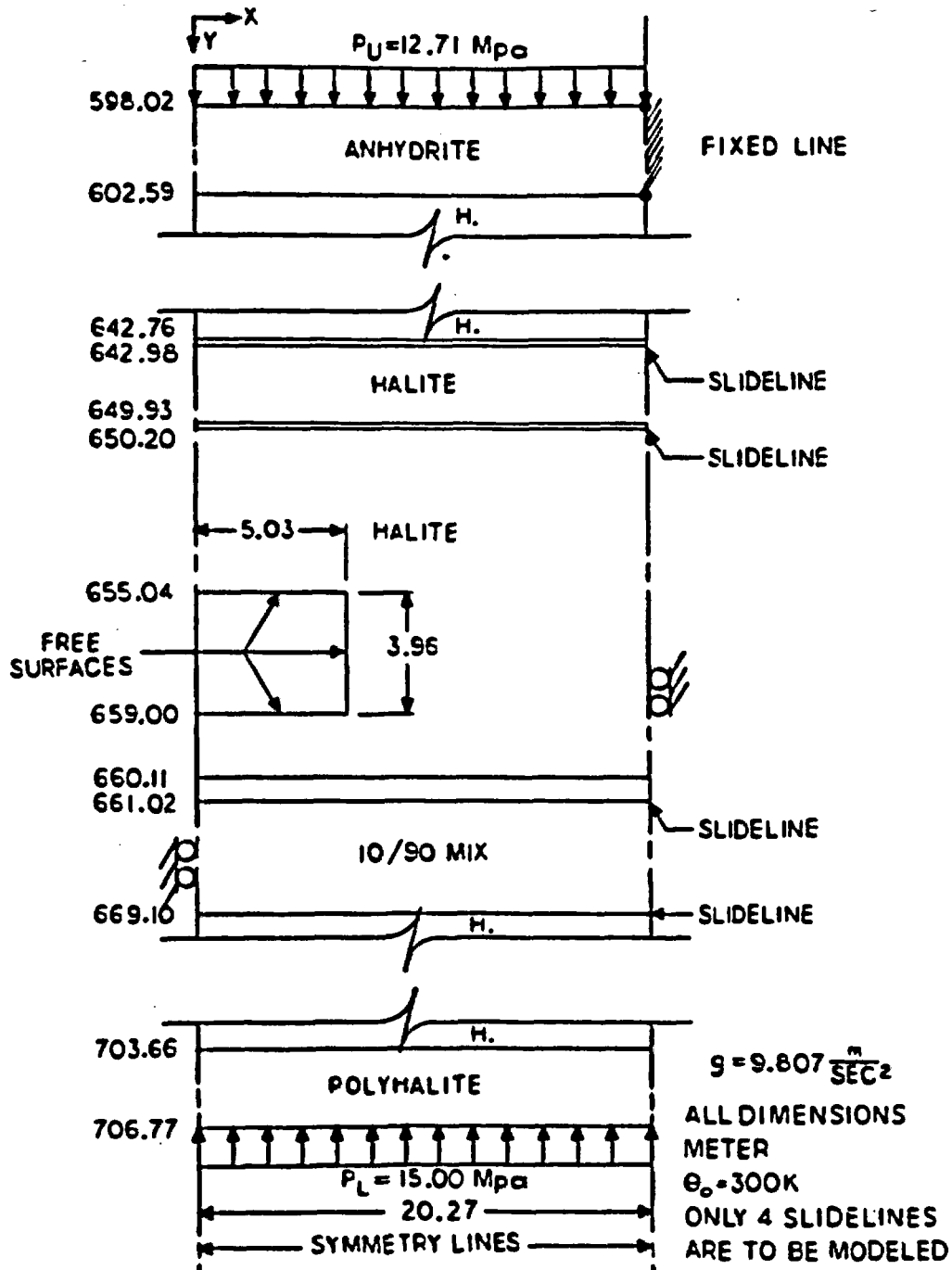


Figure 17. Problem Definition for the WIPP Benchmark II Isothermal Problem [28]

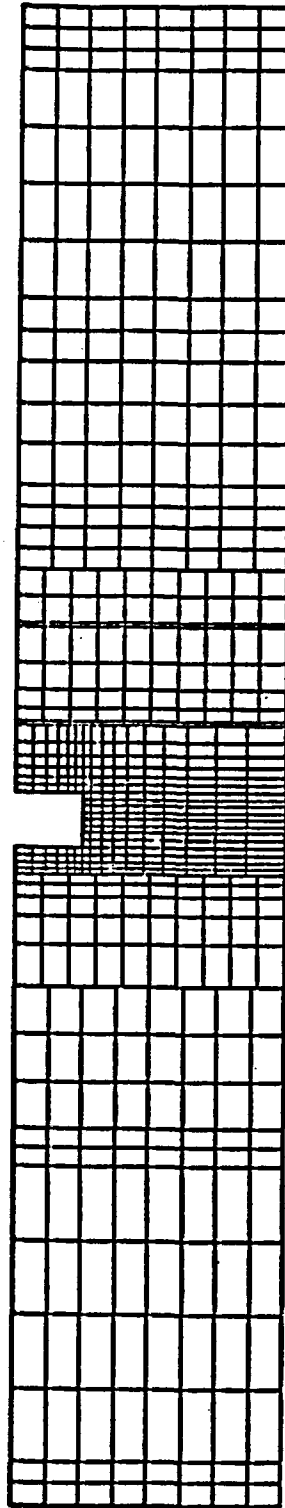


Figure 18. Mesh Used by SANCHO for the WIPP Benchmark II Isothermal Problem

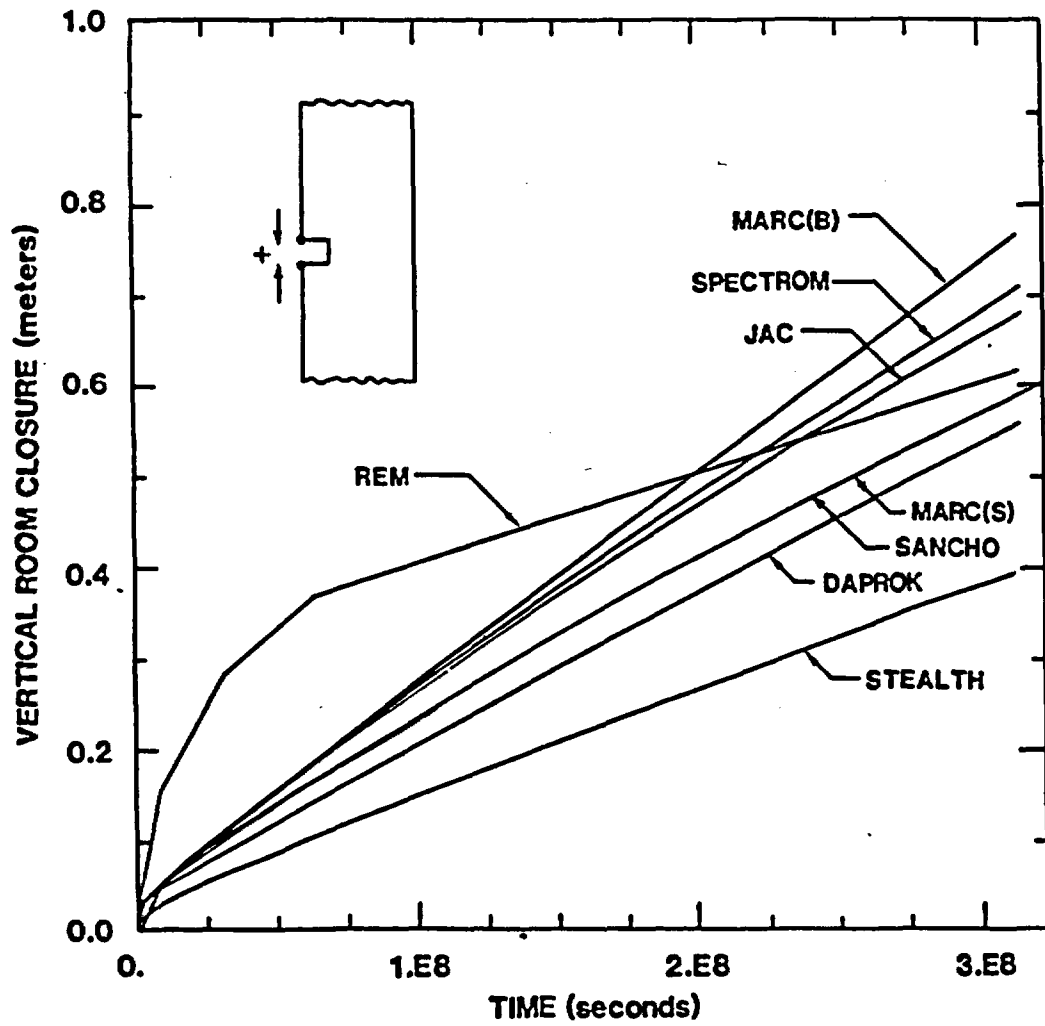


Figure 19. Closure Results for the WIPP Benchmark II [28]

PROBLEM 4

USER DEFINED INITIAL STRESS SUBROUTINE

```
SUBROUTINE INITST(ZAVG,RAVG,MX,I,BFORCE)
DIMENSION BFORCE(3)
BFORCE(1)=ZAVG*9.8066*2167.
BFORCE(2)=BFORCE(1)
BFORCE(3)=BFORCE(1)
RETURN
END
```

```
BENCHMARK 11 - SANCHO SOLUTION - CRAY I VERSION
CONTROL,4,2,.3          $ SETS STORAGE REQUIREMENTS
PLANE                   $ PLANAR PROBLEM REQUESTED
ISTRESS,VARIABLE       $ SPECIFIES INITIAL STRESS STATE
SOLUTION,5,5000,1000,.6 $ SETS CONVERGENCE AND CONTROL TOLERANCES
RESTART,33             $ SPECIFIES RESTART EVERY 33 STEPS
PLOT,ELEMENT,STRESS,STRAIN,STATE $ ELEMENT QUANTITIES WRITTEN TO TAPE
PLOT,NODAL,DISP,TEMP,RESIDUAL $ NODAL QUANTITIES WRITTEN TO TAPE
PLOT,GLOBAL,RMAG,ITER  $ GLOBAL QUANTITIES WRITTEN TO TAPE
TIMESTEP,0,330,3,157E8 $ SPECIFIES NUMBER OF TIME STEPS
TIMEPRNT,0,1,5785E7,3,157E8 $ SPECIFIES FREQUENCY OF PRINTED OUTPUT
TIMEPLOT,0,1,5785E7,3,157E8 $ SPECIFIES FREQUENCY OF PLOTTED OUTPUT
NODES                   $ ALL NODES WILL BE PRINTED
ELEMENTS                $ ALL ELEMENTS WILL BE PRINTED
ENDSET                  $ END OF SECTION ONE INPUT
MATERIAL,3,2167...-9.8066 $ MATERIAL TYPE 3
  ** HALITE **
  1.984E10,1.653E10,5.79E-36,4.9,20,13
MATERIAL,3,2167...-9.8066 $ MATERIAL TYPE 3
  ** ARGILLACEOUS HALITE **
  1.984E10,1.653E10,1.74E-35,4.9,20,13
MATERIAL,3,2167...-9.8066 $ MATERIAL TYPE 3
  ** 10 % POLYHALITE - 90 % ANHYDRITE **
  2.12E10,1.766E10,5.21E-36,4.9,20,13
MATERIAL,1,2167...-9.8066 $ MATERIAL TYPE 1
  ** POLYHALITE AND/OR ANHYDRITE **
  7.24E10,.33
ENDSET                  $ END OF SECTION TWO INPUT
PRESSURE,1,1,271E7     $ SPECIFIES PRESSURE BOUNDARY CONDITION
PRESSURE,22,1,5E7      $ SPECIFIES PRESSURE BOUNDARY CONDITION
DISPRZ,2               $ SPECIFIES ZERO DISPLACEMENT IN R AND Z
DISPR,3                $ SPECIFIES ZERO DISPLACEMENT IN R
SLIDE,4,5,0.           $ SLIDELINE SPECIFICATION
SLIDE,6,7,0.           $ SLIDELINE SPECIFICATION
SLIDE,8,9,0.           $ SLIDELINE SPECIFICATION
SLIDE,11,10,0.         $ SLIDELINE SPECIFICATION
SLIDE,16,17,-1.        $ SLIDELINE SPECIFICATION
PHISTORY,0,1,4.E8,1.   $ PRESSURE HISTORY FOR CODES 1 AND 22
END                     $ END OF INPUT DATA
```

## 7 REFERENCES

1. "MARC-CDC User Information Manual (Vols. I-III)," Publication No. 17309500, CDC Spiral Service and Publ. Dept., Minneapolis, Minn.
2. K. J. Bathe, "ADINA - A Finite Element Program for Automatic Dynamic Incremental Nonlinear Analysis, Acoustics and Vibration Laboratory, Mechanical Report 82448-1, Engineering Department, MA. Institute of Technology, Cambridge, MA, September 1975, (Revised 1977).
3. R. E. Jones, "User's Manual for QMESH, a Self-Organizing Mesh Generator Program," Sandia National Laboratories, Albuquerque, New Mexico, Report SLA-74-0239, July 1974.
4. C. Truesdell and R. A. Toupin, "The Classical Field Theories," Encyclopedia of Physics, Vol. III/1, Springer-Verlag, Berlin, 1960.
5. T. J. R. Hughes and J. Winget, "Finite Rotation Effects in Numerical Integration of Rate Constitutive Equations Arising in Large-Deformation Analysis," International Journal Numerical Methods in Engineering, 1980, Vol. 15, pp. 1862-1867.
6. J. O. Hallquist, "NIKE2D: An Implicit, Finite Deformation, Finite-Element Code for Analyzing the Static and Dynamic Response of Two-Dimensional Solids," Lawrence Livermore National Laboratory Report UCRL-52678, University of California, Livermore, March 1979.
7. J. H. Biffle, "JAC: A Two-Dimensional Finite Element Computer Program for the Non-Linear Quasistatic Response of Solids with the Conjugate Gradient Method," Sandia National Laboratories, SAND81-0998, Albuquerque, New Mexico, April 1984.
8. R. D. Krieg and S. W. Key, "Implementation of a Time Independent Plasticity Theory into Structural Computer Programs," in: J. A. Stricklin and K. J. Saczalski (eds.), Constitutive Equations in Viscoplasticity: Computational and Engineering Aspects, AMD Vol. 20, (The American Society of Mechanical Engineers, New York, 1976), pp. 125-138.
9. R. D. Krieg, "An Efficient Numerical Method for Time Independent Plasticity," SAND77-0943, Sandia National Laboratories, Albuquerque, New Mexico, November 1977.
10. R. D. Krieg and D. B. Krieg, "Accuracies of Numerical Solution Methods for the Elastic-Perfectly Plastic Model," J. Press. Vess. Tech. 99, November 1977, pp. 510-515.
11. D. Bushnell, "A Strategy for the Solution of Problems Involving Large Deflections, Plasticity and Creep," Int. J. Num. Meth's Engr., Vol. 11 (1977) pp. 683-708.
12. J. H. Argyris, L. E. Vaz and K. J. Willam, "Improved Solution Methods for Inelastic Rate Problems," Comp. Meth's Appl Mech's. and Engr. 16 (1978) pp. 231-277.

13. B. M. Irons, "Engineering Applications of Numerical Integration in Stiffness Methods," AIAA Journal, Vol. 4, No. 11, November 1968.
14. J. C. Nagtegaal, D. M. Parks and J. R. Rice, "On Numerically Accurate Finite Element Solutions in the Fully Plastic Range," Computer Methods in Applied Mechanics and Engineering, Vol. 4 (1974) pp. 153-177.
15. T. J. R. Hughes, "Equivalence of Finite Elements for Nearly-Incompressible Elasticity," LBL-5237, Lawrence Berkeley Laboratory, University of California, Berkeley, 1976.
16. T. H. H. Pian and S. W. Lee, "Notes on Finite Elements for Nearly-Incompressible Materials," AIAA Journal, Vol. 14, No. 6, June 1976, pp. 824-826.
17. J. R. H. Otter, A. C. Cassell and R. E. Hobbs, "Dynamic Relaxation," Proc. Institution of Civil Engineers, 35 (1966) pp. 633-656.
18. P. G. Underwood, "An Adaptive Dynamic Relaxation Technique for Nonlinear Structural Analysis," Lockheed Palo Alto Research Lab, LMSC-D678265, (1979), currently being revised for publication.
19. M. Papadrakakis, "A Method for the Automatic Evaluation of the Dynamic Relaxation Parameters," Computer Methods in Applied Mechanics and Engineering 25, 35-48 (1981).
20. S. W. Key, "A Finite Element Procedure for the Large Deformation Dynamic Response of Axisymmetric Solids," Computer Methods in Applied Mechanics and Engineering, 4 (1974) pp. 195-218.
21. R. E. Goodman and J. Dubois, "Duplication of Dilatancy in Analysis of Jointed Rocks," Journal of Soil Mechanics and Foundation Design, American Society of Civil Engineers, V98, 1972.
22. J. H. Biffle and R. D. Krieg, "The Solution of Quasi-Static Nonlinear Mechanics Problems by the Nonlinear Conjugate Gradient Method," ASME Special Publication, ed. T. Hughes (to be published). Presented at the ASME/ASCE Mechanics Conference, Boulder, Colorado, June 22-24, 1981.
23. S. W. Key, J. H. Biffle and R. D. Krieg, "A Study of the Computational and Theoretical Differences of Two Finite Strain Elastic-Plastic Constitutive Models," in Formules and Computational Algorithms in Finite Element Analysis, edited by Bathe, Oden, and Wunderlich, MIT, Cambridge (1977).
24. R. P. Goel and L. E. Malvern, "Biaxial Plastic Simple Waves with Combined Kinematic and Isotropic Hardening," JAM, Vol. 37, 1970, pp. 1100-1106.
25. R. D. Krieg, "A Simple Constitutive Description for Soils and Crushable Foams," SC-DR-72-0883, Sandia National Laboratories, Albuquerque, New Mexico, 1972.

26. R. D. Krieg, "Implementation of Creep Equations for a Metal Into a Finite Element Computer Program, Computer Methods for Nonlinear Solids and Structural Mechanics, ASME Special Publication AMD Vol. 54, 1983.
27. W. Prager and P. G. Hodge, Theory of Perfectly Plastic Solids, John Wiley and Sons, New York, 1963.
28. Harold S. Morgan, Raymond D. Krieg, and Rudolph V. Matalucci, Comparative Analysis of Nine Structural Codes Used in the Second WIPP Benchmark Problem, SAND81-1389, Sandia National Laboratories, Albuquerque, New Mexico, November 1981.
29. Z. E. Beisinger, SEACO: Sandia Engineering Analysis Department Code Output Data Base, SAND84-2004, Sandia National Laboratories, Albuquerque, New Mexico, in press.

**DISTRIBUTION:**

U.S. Department of Energy, Headquarters  
Office of Nuclear Waste Management  
Washington, D.C. 20545  
A. Follett, Project Coordinator (WIPP) (1)  
R. Stein

U.S. Department of Energy, Albuquerque Operations  
P.O. Box 5400  
Albuquerque, NM 87185  
G. C. Romatowski  
W. R. Cooper, WIPP Project Office, (Carlsbad) (2)  
D. G. Jackson, Director, Public Affairs Division  
A. Hunt, WPO (Carlsbad) (4)

U.S. Department of Energy  
Carlsbad WIPP Project Office  
Room 113, Federal Building  
Carlsbad, NM 88220

U.S. Department of Energy, NPO  
Office of Nuclear Waste Isolation  
505 King Avenue  
Columbus, OH 43201  
Jeff O. Neff  
R. Wunderlich

U.S. Nuclear Regulatory Commission  
Division of Waste Management  
Mail Stop 697SS  
Washington, D.C. 20555  
Michael Bell  
Hubart Miller

Battelle Memorial Institute  
Project Management Division  
505 King Avenue  
Columbus, OH 43201  
W. Carbiener, General Manager (3)  
S. Basham  
D. E. Clark  
S. Goldsmith  
J. E. Hanley  
P. Hoffman  
H. R. Hume  
H. N. Kalia  
J. Kircher  
S. Matthews  
D. Moak  
J. Moody  
G. Raines  
J. Treadwell  
ONWI Library

Westinghouse Electric Corporation  
P.O. Box 40039  
Albuquerque, NM 87196  
P. Miskimin  
V. Likar

Bechtel, Inc.  
P.O. Box 3965  
45-11-B34  
San Francisco, CA 94119  
E. Weber  
D. Roberts  
H. Taylor  
P. Frobenius  
C. L. Wu  
D. L. Wu  
N. Antonas  
W. T. Li  
B. R. Chytrowski

National Academy of Sciences, WIPP Panel  
Konrad B. Krauskopf, Chairman  
Department of Geology  
Stanford University  
Stanford, CA 94305

Frank L. Parker, Vice Chairman  
Department of Environmental and  
Water Resources Engineering  
Vanderbilt University  
Nashville, TN 37235

Dr. Karl P. Cohen, Member  
928 N. California Avenue  
Palo Alto, CA 94303

Fred M. Ernsberger, Member  
205 Old Mill Road  
Pittsburgh, PA 15238

Dr. Harold James, Member  
1617 Washington Street  
Port Townsend, WA 98368

Richard R. Parizek, Member  
Department of Hydrogeology  
Pennsylvania State University  
University Park, PA 16802

D'Arcy A. Shock, Member  
233 Virginia  
Ponca City, OK 74601

John W. Winchester, Member  
Department of Oceanography  
Florida State University  
Tallahassee, FL 32306

National Academy of Sciences  
Committee on Radioactive Waste Management  
2101 Constitution Avenue, NW  
Washington, D.C. 20418  
John T. Holloway, Senior Staff Officer

Hobbs Public Library  
509 N. Ship Street  
Hobbs, NM 88248  
Ms. Marcia Lewis, Librarian

New Mexico Tech  
Martin Speere Memorial Library  
Campus Street  
Socorro, NM 87810

New Mexico State Library  
P.O. Box 1629  
Santa Fe, NM 87503  
Ms. Ingrid Vollenhofer

Zimmerman Library  
University of New Mexico  
Albuquerque, NM 87131  
Zanier Vivian

WIPP Public Reading Room  
Atomic Museum, Kirtland East AFB  
Albuquerque, NM 87185  
Ms. Gwynn Schreiner

WIPP Public Reading Room  
Carlsbad Municipal Library  
101 S. Hallagueno Street  
Carlsbad, NM 88220  
Lee Hubbard, Head Librarian

Thomas Brannigan Library  
106 W. Hadley Street  
Las Cruces, NM 88001  
Don Dresp, Head Librarian

Roswell Public Library  
301 N. Pennsylvania Avenue  
Roswell, NM 88201  
Ms. Nancy Langston

State of New Mexico  
Environmental Evaluation Group  
320 Marcy Street  
P.O. Box 968  
Santa Fe, NM 87503  
Robert H. Neill, Director (2)

NM Department of Energy & Minerals  
P.O. Box 2770  
Santa Fe, NM 87501  
Larry Kehoe, Secretary  
Kasey LaPlante, Librarian

Institut für Tiemplagerung  
Theodor-Heuss-Strasse 4  
D-3300 Braunschweig  
Federal Republic of Germany  
K. Kuhn  
N. Jockwer  
H. Gies

Michael Langer  
Bundesanstalt für Geowissenschaften  
und Rohstoffe  
Postfach 510 153  
3000 Hannover 51  
Federal Republic of Germany

Klaus Eckart Maass  
Hahn-Meitner-Institut für Kernforschung  
Glienicke Strasse 100  
1000 Berlin 39  
Federal Republic of Germany

Rolf-Peter Randl  
Bundesministerium für Forschung und  
Technologie  
Postfach 200 706  
5300 Bonn 2  
Federal Republic of Germany

Helmut Rothemeyer  
Physikalisch-Technische Bundesanstalt  
Bundesanstalt 100, 3300 Braunschweig  
Federal Republic of Germany

Dr. Paul R. Dawson  
254 Upson Hall  
Dept. Mech. & Aerospace Engr.  
Cornell University  
Ithaca, NY 14853

RE/SPEC Inc.  
P.O. Box 725  
Rapid City, SD 57701  
Attn: Dr. P. Gnirk  
A. Fossum

RE/SPEC Inc.  
P.O. Box 14984  
Albuquerque, NM 87191  
Attn: S. W. Key

Los Alamos Scientific Laboratory (2)  
P. O. Box 1663  
Los Alamos, NM 87545  
Attn: C. A. Anderson, Q-13, MC-576  
J. J. Ruminer, WX-3, MC-931

Massachusetts Institute of Technology  
Department of Mechanical Engineering  
Cambridge, MA 02139  
Attn: K. J. Bathe, Room 3-356

Northwestern University  
Department of Engineering  
Technological Institute  
Evanston, IL 60201  
Attn: T. Belytschko

ANATECH  
3344 N. Torrey Pines Ct.  
Suite 320  
La Jolla, CA 92037  
Attn: R. S. Dunham

University of Washington  
Mechanical Engineering Department  
Seattle, WA 98105  
Attn: A. Emery

University of Arizona  
Tucson, AZ 85721  
Attn: R. H. Gallagher  
Dean of Engineering

University of California  
Lawrence Livermore Laboratory  
P. O. Box 808  
Livermore, CA 94550  
Attn: G. L. Goudreau, L-122  
J. O. Hallquist, L-122

University of New Mexico  
Department of Civil Engineering  
Albuquerque, NM 87131  
Attn: R. Johnson

Brigham Young University  
Civil Engineering Department  
Provo, UT 84602  
Attn: S. E. Benzley

Argonne National Laboratory  
Reactor Analysis and Safety Division  
9700 South Cass Avenue  
Argonne, IL 60439  
Attn: J. M. Kennedy

Stanford University  
Division of Applied Mechanics  
Department of Mechanical Engineering  
School of Engineering  
Stanford, CA 94305  
Attn: T. J. R. Hughes

University of California  
Division of Structural Engineering and  
Structural Mechanics  
Department of Civil Engineering  
Berkeley, CA 94720  
Attn: R. Taylor, Rm 705, Davis Hall

Massachusetts Institute of Technology  
Aeroelastic and Structures Research  
Laboratory  
Department of Aeronautics and Astronautics  
Cambridge, MA 02139  
Attn: E. A. Witmer, Director

GWU-NASA Langley Research Center  
Hampton, VA 23665  
Attn: A. R. Noor, MS 246

University of Texas at Austin  
Department of Aerospace Engineering  
and Engineering Mechanics  
Austin, TX 78712  
Attn: J. T. Oden  
E. B. Becker

Applied Science and Technology  
3344 N. Torrey Pines Ct.  
Suite 320  
La Jolla, CA 92037  
Attn: R. E. Nickell

Sandy Figuers  
12018 Dorrance  
Stafford, Tx 77477

SANDIA INTERNAL

0313 J. T. Schamaun  
1510 J. W. Nunziato  
1511 G. G. Weigand  
1511 D. K. Gartling  
1520 D. J. McCloskey  
1521 R. D. Krieg (10)  
1521 Z. E. Beisinger (10)  
1521 S. N. Burchett  
1521 H. S. Morgan  
1521 D. S. Preece  
1521 C. M. Stone (25)  
1521 G. D. Sjaardema  
1522 R. C. Reuter  
1522 E. P. Chen  
1523 J. H. Biffle  
1523 C. H. Conley  
1523 D. P. Flanagan  
1524 W. N. Sullivan  
1524 L. J. Branstetter  
1524 K. W. Schuler  
1524 L. M. Taylor  
1530 L. W. Davison  
1531 S. L. Thompson  
1531 T. Canfield  
1533 P. Yarrington  
1533 S. T. Montgomery  
1534 J. R. Asay  
Attn: T. G. Trucano  
1540 W. C. Luth  
1542 B. M. Butcher  
1542 L. S. Costin

1642 L. F. Shampine  
 Attn: B. L. Hulme  
 1813 J. G. Curro  
 Attn: E. D. Reedy  
 1832 W. B. Jones  
 Attn: R. J. Bourcier  
 3141 L. J. Erickson (Library ) (5)  
 3151 W. L. Garner, For: DOE/TIC (Unlimited Release) (3)  
 3154-4 C. Dalin, For: DOE/TIC (25)  
 3310 W. D. Burnett  
 6000 E. H. Beckner  
 6257 J. K. Linn  
 Attn: R. R. Beasley  
 6258 P. J. Hommert  
 Attn: R. L. Parrish  
 B. J. Thorne  
 6300 R. W. Lynch  
 6310 T. O. Hunter  
 Attn: L. W. Scully, 6311  
 J. R. Tillerson, 6313  
 6330 W. D. Weart  
 6332 L. D. Tyler  
 6332 R. Beraun  
 6332 R. V. Matalucci  
 6332 D. E. Munson  
 6332 J. C. Stormont  
 6332 T. M. Torres  
 6332 Sandia WIPP Central Files (HLW) (2)  
 6442 W. A. Von Rieseemann  
 8231 R. J. Kee  
 8240 C. W. Robinson  
 8241 G. A. Benedetti  
 8241 M. L. Chiesa  
 8241 J. C. Keilman  
 8241 L. E. Voelker  
 8242 M. L. Callabresi  
 8242 J. E. Grant  
 8242 W. E. Mason  
 8242 L. M. Napolitano  
 8242 L. I. Weingarten  
 8243 M. R. Birnbaum  
 8243 D. J. Bammann  
 8243 N. D. Gilbertson  
 8316 T. C. Lowe